6706 J. Med. Chem. 2010, 53, 6706–6719
DOI: 10.1021/jm100814g

Journal of Medicinal Chemistry Article

Design, Synthesis, and Biological Evaluation of Halogenated *N*-(2-(4-Oxo-1-phenyl-1,3,8-triazaspiro[4.5]decan-8-yl)ethyl)benzamides: Discovery of an Isoform-Selective Small Molecule Phospholipase D2 Inhibitor

Robert R. Lavieri,[‡,†] Sarah A. Scott,[‡,†] Paige E. Selvy,[‡] Kwangho Kim,[∥] Satyawan Jadhav,[‡] Ryan D. Morrison,[⊥] J. Scott Daniels,[‡,⊥] H. Alex Brown,[‡,§,∥] and Craig W. Lindsley*[,‡,§,∥,⊥]

[‡]*Department of Pharmacology,* [§]*Department of Chemistry,* [∥]*Vanderbilt Institute of Chemical Biology, and* [⊥]*Vanderbilt Program in Drug Discovery, Vanderbilt University Medical Center, Nashville, Tennessee 37232-6600.* [†]*These authors contributed equally to this work.*

Received July 1, 2010

Phospholipase D (PLD) catalyzes the conversion of phosphatidylcholine to the lipid second messenger phosphatidic acid. Two mammalian isoforms of PLD have been identified, PLD1 and PLD2, which share 53% sequence identity and are subject to different regulatory mechanisms. Inhibition of PLD enzymatic activity leads to increased cancer cell apoptosis, decreased cancer cell invasion, and decreased metastasis of cancer cells; therefore, the development of isoform-specific, PLD inhibitors is a novel approach for the treatment of cancer. Previously, we developed potent dual PLD1/PLD2, PLD1-specific (>1700-fold selective), and moderately PLD2-preferring (>10-fold preferring) inhibitors. Here, we describe a matrix library strategy that afforded the most potent (PLD2 IC_{50} = 20 nM) and selective (75-fold selective versus PLD1) PLD2 inhibitor to date, *N*-(2-(1-(3-fluorophenyl)-4-oxo-1,3,8-triazaspiro[4.5]decan-8-yl)ethyl)-2-naphthamide (**22a**), with an acceptable DMPK profile. Thus, these new isoform-selective PLD inhibitors will enable researchers to dissect the signaling roles and therapeutic potential of individual PLD isoforms to an unprecedented degree.

Introduction

Cancer is the second leading cause of mortality in the United States.[1] Both academic and industrial groups have expended significant effort in attempts to develop novel chemotherapeutics and, more recently, to identify previously underappreciated targets essential to disease progression. Advancing our basic understanding of cancer as a molecular phenomenon through the use of small molecules is an important mechanism by which to both identify new targets and develop innovative cancer therapeutics. Historically, targeted cancer drug discovery efforts have focused on the development of small molecule kinase inhibitors (typically at the ATP binding site, though allosteric inhibitors are emerging) due to the central role many kinases play in regulating cell growth and division. The development of kinase inhibitors into drugs has been partially hindered by poor selectivity versus the more than 500 members of the human kinome. The identification of other protein targets that regulate cell survival, invasion, and proliferation will provide alternative options for cancer drug development.

PLD[a] catalyzes the hydrolysis of phosphatidylcholine (PC, **1**) into the lipid second messenger phosphatidic acid (PA, **2**) and choline **3** (Figure 1).[2] PA is an essential lipid second messenger that is strategically located at the intersection of several essential signaling and metabolic pathways.[3] Increased PLD expression and aberrant PLD enzymatic activity have been observed in a variety of human cancers including breast cancer,[4] renal cancer,[5] colorectal cancer,[6] and glioblastoma.[7] Additionally, PLD activity has been shown to be required for mutant Ras driven tumorigenesis in mice.[8] Experiments utilizing inactivating mutations of PLD suggest that inhibiting PLD enzymatic activity decreases cancer cell invasion[9] and increases apoptosis.[10] On a molecular level PLD has been implicated in oncogenic signaling events involving the epidermal growth factor receptor (EGFR),[11] matrix metalloproteinase (MMP) secretion,[7,12] p53,[13,14] the mammalian target of rapamycin (mTOR),[15,16] and Ras.[17] Taken together, evidence from genetic and biochemical experiments indicates that PLD is an attractive target for cancer therapy. Until recently, the tools available to inhibit PLD activity were limited to genetic and biochemical approaches including the use of 1-butanol, none of which are viable therapeutic options. Furthermore, 1-butanol is not a PLD inhibitor; rather 1-butanol blocks PLD-catalyzed phosphatidic acid production by competing with water as a nucleophile, thereby causing the formation of phosphatidylbutanol **4** in a unique transphosphatidylation reaction.[2] Several *pan*-PLD inhibitors **5**−**11** have been reported,[18−24] but many of these compounds do not act directly on the enzyme, lack target potency, or are not drug-like molecules (Figure 2A). Developing isoform-selective PLD inhibitors is a formidable task due to several factors: (1) PLD1 and PLD2 are challenging to purify in large quantities, (2) the enzyme activity assays are labor intensive and

*To whom correspondence should be addressed. E-mail: craig.lindsley@vanderbilt.edu. Phone: 615-322-8700, Fax: 615-343-6532.

[a] Abbreviations: PA, phosphatidic acid; PC, phosphatidylcholine; PLD, phospholipase D; EGFR, epidermal growth factor receptor; mTOR, mammalian target of rapamycin; gfp, green fluorescence protein; PAM, positive allosteric modulator; NAM, negative allosteric modulator; FBS, fetal bovine serum.

 Published on Web 08/24/2010

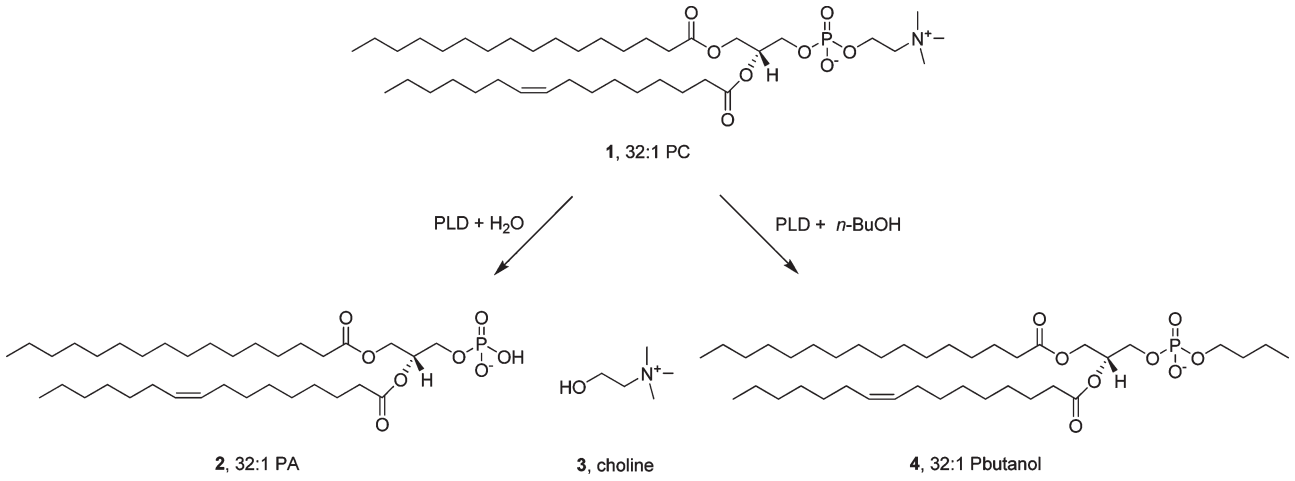

Figure 1. PLD catalyzed the hydrolysis of phosphatidylcholine **1** (PC) into phosphatidic acid **2** (PA) and choline **3**. In the presence of a primary alcohol, typically 1-butanol, PLD catalyzes a unique transphosphatidylation reaction to produce phosphatidylbutanol **4**.

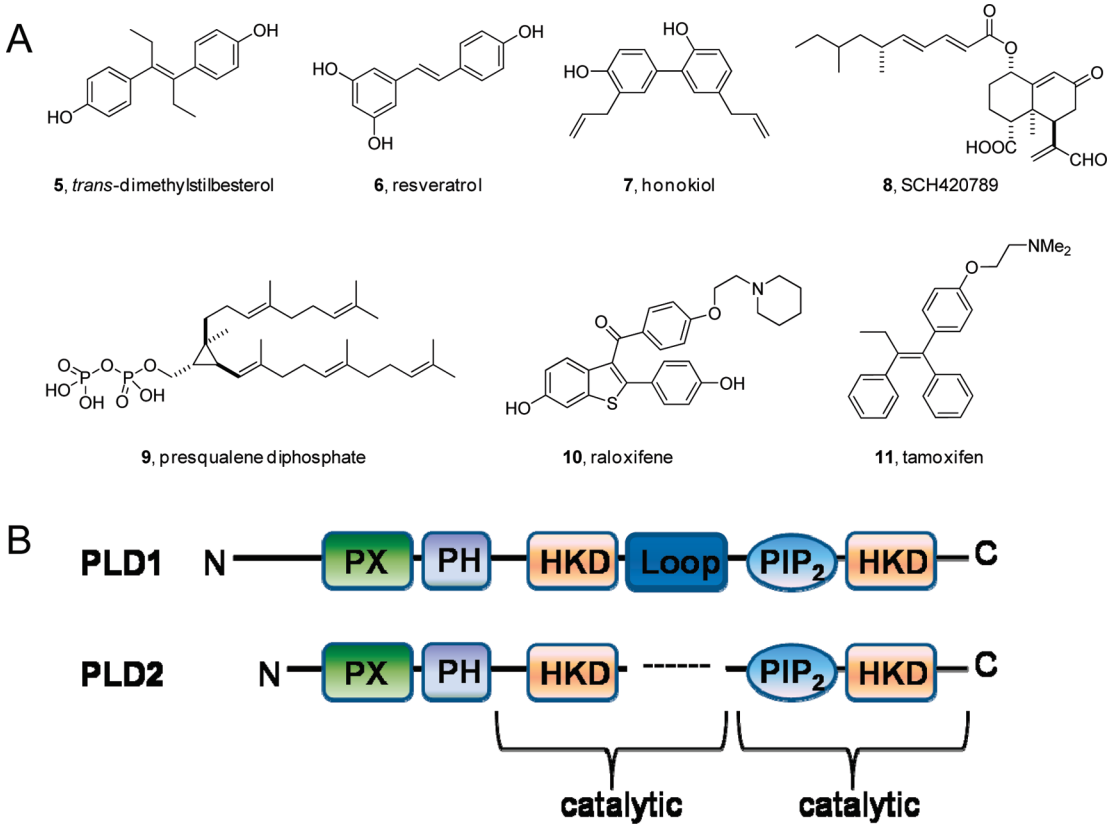

Figure 2. (A) Structures of reported PLD inhibitors. (B) Sequence of PLD1 and PLD2 highlighting the PX and PH domains, the two HKD motifs, the two catalytic sites, and the loop in PLD1, which is absent in PLD2. Overall, homology between the two PLD isoforms is only 53%.

time-consuming, and (3) the two mammalian isoforms of PLD share 53% sequence identity (Figure 2B). Importantly, due to the multitude of cellular events which require PA ablating all PLD enzymatic activity may not be a viable therapeutic approach, in which case it would be necessary to possess isoform-selective PLD inhibitors.

A turning point for the field occurred in 2007, when a group at Novartis disclosed halopemide **12** as a PLD2 inhibitor discovered in a high-throughput screen;[25] however, rigorous characterization by our laboratories demonstrated that **12** and the reported analogues were dual PLD1/2 inhibitors or even moderately PLD1 preferring (Figure 3).[26] Nonetheless, this was the first time a potent, direct-acting, drug-like, small-molecule PLD inhibitor had been reported; therefore, we began a campaign to optimize halopemide for isoform-specific PLD inhibition. An initial diversity-oriented synthesis approach yielded a library of 263 compounds containing direct-acting, potent (IC_{50} values 1−50 nM) PLD1 inhibitors, such as **13** with 160-fold selectivity versus PLD2 in cellular enzyme activity assays.[26] A subsequent iterative analogue synthesis approach delivered **14** with improved PLD1 potency (IC_{50} = 3.7 nM) and selectivity (>1700-fold selective versus PLD2 in cells).[27] The identification of a single chiral (*S*)-methyl group provided a significant gain in PLD1 selectivity.

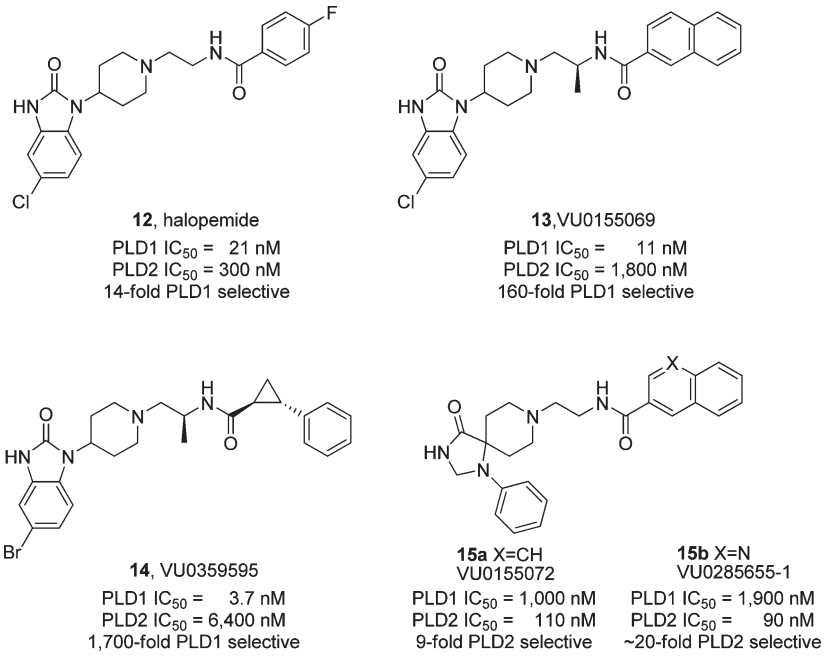

Figure 3. Structures and activities of halopemide **12** and isoform-selective PLD inhibitors **13** and **14** (PLD1 selective) and **15a**,**b** (PLD2 preferring).

Developing a PLD2-selective inhibitor has been significantly more challenging. After synthesizing over 500 compounds, we identified a 1,3,8-triazaspiro[4,5]decan-4-one scaffold that engendered PLD2-preferring inhibition, with the best compound, **15b**, only possessing ~20 fold selectivity for PLD2 in cells (Figure 3).[28] Studies with various PLD constructs suggest that these inhibitors may bind at an allosteric site in the N-terminus, accounting for the high isoform selectivity and unique, shallow SAR.[26] Moreover, these inhibitors blocked the in vitro invasive migration of a triple negative breast cancer cell line (MDA-MB-231), and siRNA studies indicated that PLD2 played a dominant role.[26]

Due to a lack of small molecule tools and a perception of phospholipases as nondruggable targets coupled with labor intensive and complex assay systems, little effort has been focused on their therapeutic potential. Herein we discuss our ongoing medicinal chemistry efforts to develop isoform-selective phospholipase D (PLD) inhibitors, the development of the first PLD2-selective inhibitor, and the potential for PLD inhibitors as a new class of cancer therapeutics. Here, we report the results of our a matrix library approach to increase PLD2 potency and selectivity within the 1,3,8-triazaspiro-[4,5]decan-4-one series.

Chemistry

Previous work showed that SAR was shallow with respect to the Eastern amide moiety in **15a**,**b**;[28] thus current efforts focused on functionalization of the 1,3,8-triazaspiro[4,5]decan-4-one scaffold by the incorporation of various halogens, as this proved successful in the benzimidazolone-based PLD1 inhibitors **13** and **14**.[27] Only the unsubstituted 1-phenyl-1,3,8-triazaspiro[4,5]decan-4-one was commercially available, so while known in the literature, the halogenated congeners had to be synthesized. As shown in Scheme 1, *N*-benzylpiperidinone **16** underwent a Strecker reaction with 3-fluoroaniline to provide **17a**, and acidic hydrolysis delivered the carboxamide **18a** in 68% yield for the two steps. Closing of the spirocyclic five-membered ring required forcing microwave-assisted conditions (150 °C for 15 min in AcOH), followed by reduction to provide **19a** in 12% yield. A final hydrogenation with Pd/C removed the benzyl protecting group, affording the key scaffold **20a** in 96% yield. In a similar manner, key scaffolds **20b**−**f** were prepared in overall yields from **16** averaging 8%.

Scheme 1[a]

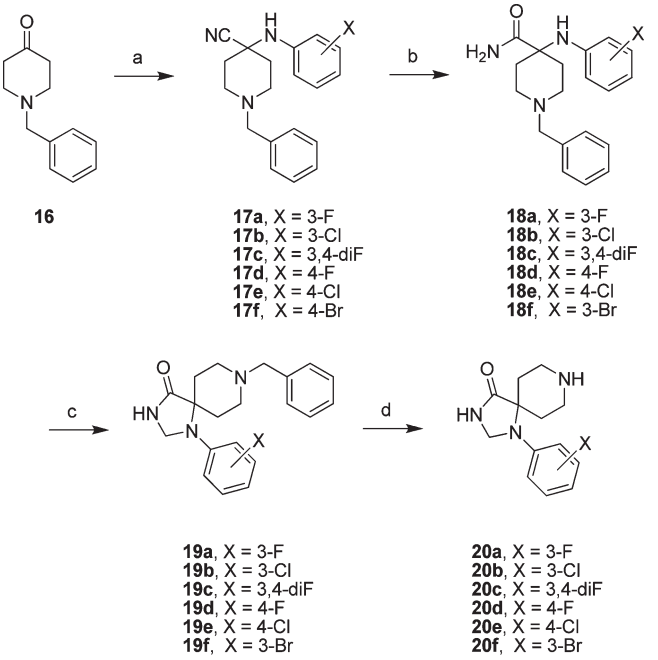

[a] Reagents and conditions: (a) KCN, AcOH, $ArNH_2$, 12 h, room temperature; (b) H_2SO_4, 12 h, 68%−74% for two steps; (c) (i) trimethyl orthoformate, AcOH, microwave, 150 °C, 15 min; (ii) $NaBH_4$, MeOH, 3 h, 12%−20%; (d) H_2, Pd/C, MeOH, AcOH, 20 h, 89%−96%.

With the requisite synthetically derived halogenated congeners **20a**−**f** in hand, we initiated the synthesis of a 4 × 6 matrix library of 24 analogues based on the PLD2-preferring

Scheme 2[a]

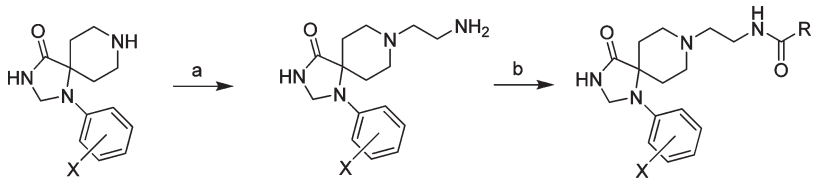

20a, X = 3-F
20b, X = 3-Cl
20c, X = 3,4-diF
20d, X = 4-F
20e, X = 4-Cl
20f, X = 4-Br

21a, X = 3-F
21b, X = 3-Cl
21c, X = 3,4-diF
21d, X = 4-F
21e, X = 4-Cl
21f, X = 4-Br

22, X = 3-F
23, X = 3-Cl
24, X = 3,4-diF
25, X = 4-F
26, X = 4-Cl
27, X = 4-Br

[a] Reagents and conditions: **22(a-f)** − **27(a-f)** (a) (i) *tert*-butyl 2-oxoethylcarbamate, MP-B(OAc)$_3$H, DCM, MeOH, 18 h, (ii) 4.0 M HCl/dioxane, DCM, MeOH, 4 h, 58%−78%; (b) RCOCl, DIEA, DMF, room temperature, 4 h, 75%−85%.

Table 1. Structures and Cellular Assay Activities of Analogues **22a−d−27a−d**

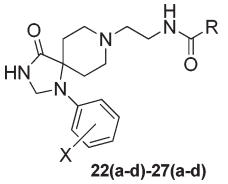

22(a-d)-27(a-d)

Cmpd	X	R	PLD1 IC_{50} (nM)[a]	PLD2 IC_{50} (nM)[b]	Fold PLD2 Selective
22a	3-F	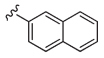	1,500	20	75
22b	3-F	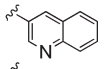	2,500	63	40
22c	3-F	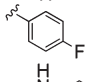	12,000	6,700	1.8
22d	3-F	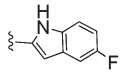	210	25	8
23a	3-Cl	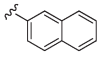	1,200	290	4
23b	3-Cl	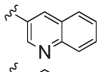	870	165	5
23c	3-Cl	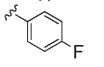	3,470	70	50
23d	3-Cl	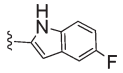	250	73	3.4
24a	3,4-diF	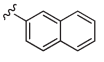	2,800	120	23
24b	3,4-diF	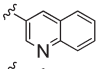	2,060	70	30
24c	3,4-diF	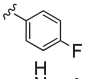	5,780	660	9
24d	3,4-diF	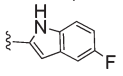	390	100	4
25a	4-F	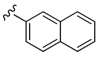	1,700	80	21
25b	4-F	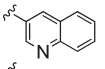	2,000	40	50
25c	4-F	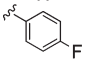	14,000	610	23
25d	4-F	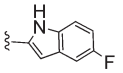	290	30	9
26a	4-Cl	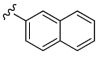	2,270	655	3.5
26b	4-Cl	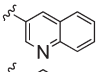	3,500	200	17
26c	4-Cl	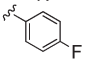	5,590	5,670	~1
26d	4-Cl	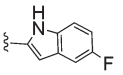	335	50	7
27a	4-Br	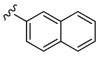	5,900	350	17
27b	4-Br	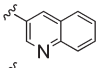	2,700	360	8
27c	4-Br	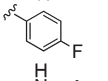	10,000	8,000	~1
27d	4-Br	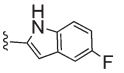	2,660	100	27

[a] Cellular PLD1 assay with Calu-1 cells. [b] Cellular assay with HEK293-gfpPLD2 cells. Cell-based assays were used to develop CRCs (from 200 pM to 20 μM) and determine IC_{50}s for all compounds in Calu-1 or HEK293-gfpPLD2 cell lines. The geometric mean of the standard errors of the log(IC_{50}) values from the curve fits of all compounds were computed and compared to the IC_{50}s themselves. There were levels of ~30% error for Calu-1 and ~70% for HEK293-gfpPLD2 IC_{50}s. Despite the variance in the absolute values over a large number of assays, the reproducibility of the effects and relative potency of the inhibitors were found to be robust.

inhibitors **15a**,**b** (Scheme 2). In the event, 1,3,8-triazaspiro-[4,5]decan-4-ones **20a−f** underwent a reductive amination reaction with *tert*-butyl 2-oxoethylcarbamate to provide, after deprotection, amines **21a−f** in 58−78% yields. Then, the six amines **21a−f** were acylated with four acid chlorides (2-naphthyl, 3-quinolyl, 4-fluorobenzoyl, and 5-fluoro-2-indolyl) to deliver the 24-member library of analogues **22a−d−27a−d** in 75%−85% yields. All final compounds were purified by mass-directed preparative HPLC to analytical purity.

Results and Discussion

All library members **22a**−**d**−**27a**−**d** were evaluated for their ability to inhibit PLD1 and PLD2 in a cellular assay (Calu-1 and HEK293-gfpPLD2 cell lines, respectively) as well as a biochemical assay with recombinant PLD1 and PLD2 enzymes. The cellular assays were the "workhorse" assays that drove the SAR, with routine confirmation in the in vitro biochemical assay to ensure compounds were direct acting inhibitors. As shown in Table 1, SAR for the 24-member library marked a clear departure from the SAR of the earlier PLD1-selective benzimidazolone-based inhibitors, and all but two of the analogues **22a**−**d**−**27a**−**d** displayed a preference for PLD2 inhibition, with the two exceptions, **26c** and **27c**, being dual PLD1/2 inhibitors with comparable PLD1 and PLD2 inhibition. Both PLD2 potency and selectivity were dependent on the halogen employed, the substitution pattern on the phenyl ring of the 1,3,8-triazaspiro[4,5]decan-4-one scaffold, and the nature of the eastern amide moiety. As with many allosteric ligands, SAR was shallow and unpredictable. However, this matrix library approach identified several PLD2 inhibitors that represented a significant improvement over the original PLD2 inhibitor **15a** and highlights the power and utility of a matrix library approach, as the SAR would not have informed a singleton approach toward optimal PLD2 inhibitors. For example, **23c** and **25b** displayed ~50-fold selectivity for PLD2, with PLD2 IC_{50}s of 70 and 40 nM, respectively; interestingly, **23c** contains the 3-Cl moiety and a 4-fluorphenyl amide whereas **25b** is based on a 4-F scaffold and a 3-quinolinyl amide. Any other combination within these scaffolds results in a decrease in either PLD2 potency or PLD2 selectivity. From this effort, we discovered the most potent and selective PLD2 inhibitor to date, **22a** (VU0364739), with a PLD2 IC_{50} of 20 nM and possessing 75-fold selectivity versus PLD1 in the cellular assay (Figure 4A). In our in vitro biochemical assay using purified PLD1 and PLD2, **22a** possessed a PLD1 IC_{50} of 7500 nM and a PLD2 IC_{50} of 100 nM, replicating the unprecedented 75-fold selectivity for PLD2 (Figure 4B). While we could not replicate the fortuitous 1700-fold PLD1 selectivity of **14** in a PLD2-preferring inhibitor, the 75-fold PLD2 selectivity of **22a** afforded a small molecule probe to effectively evaluate PLD2 pharmacology. With potent and isoform-selective PLD1 (**14**) and PLD2 (**22a**) inhibitors in hand, we were poised to dissect the individual roles of PLD1 and PLD2 in a number of in vitro cancer cell models.

In our earlier work with PLD1 inhibitor **13** and the moderately selective PLD2 inhibitor **15a**, we found that both inhibitors blocked the in vitro invasive migration of a triple negative breast cancer cell line (MDA-MB-231); however, siRNA studies indicated that PLD2 played a dominant role.[26] With significantly improved isoform-selective PLD1 (**14**) and PLD2 (**22a**) inhibitors, we extended our study to dissect the roles of PLD1 and PLD2 for proliferation and apoptosis in MDA-MB-231 breast cancer cells. PLD2 inhibitor **22a** provided a striking effect in a 48 h cell proliferation assay, wherein inhibition of PLD2 affords a pronounced decrease in cell proliferation of MDA-MB-231 cells, as compared to an equivalent 10 μM concentration of the PLD1 inhibitor **14** (Figure 5A). When cultured under serum-free conditions, the same assay in MDA-MB-231 cells resulted in almost a complete blockade of proliferation with **22a**, and under these conditions, PLD1 inhibition has a significant effect as well (Figure 5B). These data do show a preferential sensitization of

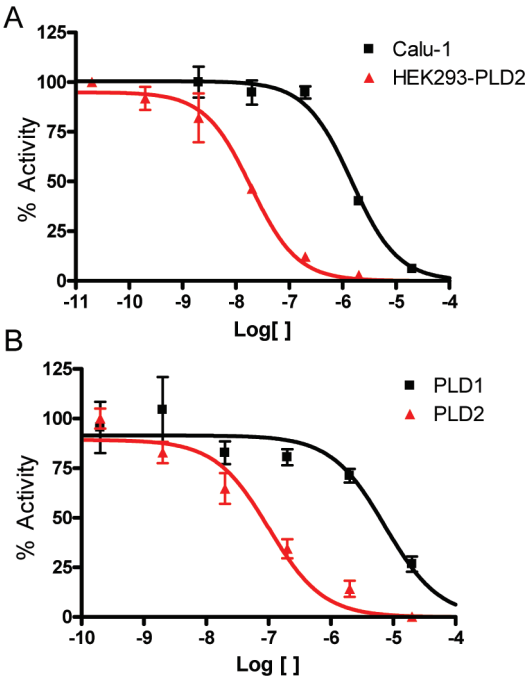

Figure 4. Concentration−response curves (CRCs) for (A) cellular PLD1 (■) (Calu-1) assay and PLD2 (▲) (HEK293-gfpPLD2) assay and (B) biochemical inhibition assay CRCs with purified (■) PLD1 and (▲) PLD2 highlighting the unprecedented 75-fold PLD2 versus PLD1 selectivity for **22a** in both PLD assays. Error bars show standard error of the mean for triplicate measurements.

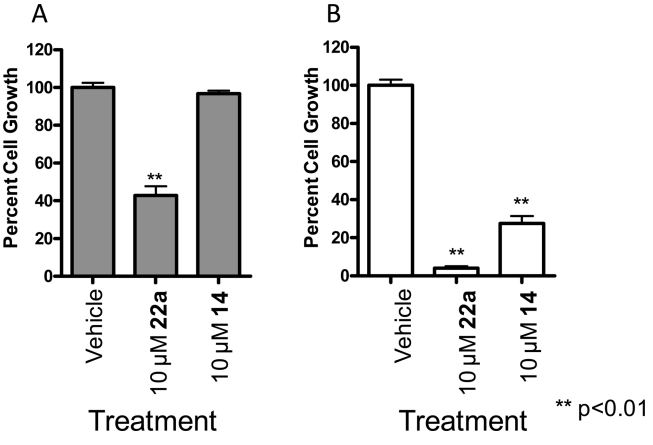

Figure 5. Inhibition of PLD2 with **22a** leads to decreased proliferation of MDA-MB-231 cells. MDA-MB-231 cells were cultured in the presence of PLD inhibitor for 48 h after which cell viability was assayed using WST-1 cell proliferation reagent. (A) MDA-MB-231 cells cultured in the presence of 10% FBS were fairly resistant to PLD inhibitor treatment with only 10 μM **22a** treatment leading to a significant decrease in cell proliferation. (B) MDA-MB-231 cells cultured under serum-free conditions had a more pronounced response to PLD inhibition with both PLD1- (**14**) and PLD2- (**22a**) selective compounds significantly decreasing cell proliferation. $n = 3$. Error bars show standard error of the mean for triplicate measurements.

MDA-MB-231 cells to PLD2 inhibition. There was a noticeable difference in the effect of PLD inhibitor treatment on MDA-MB-231 cell proliferation depending on culture conditions. When cells were cultured in the absence of serum with either inhibitor **14** or **22a**, there was a more pronounced decrease in cell growth compared to the vehicle control

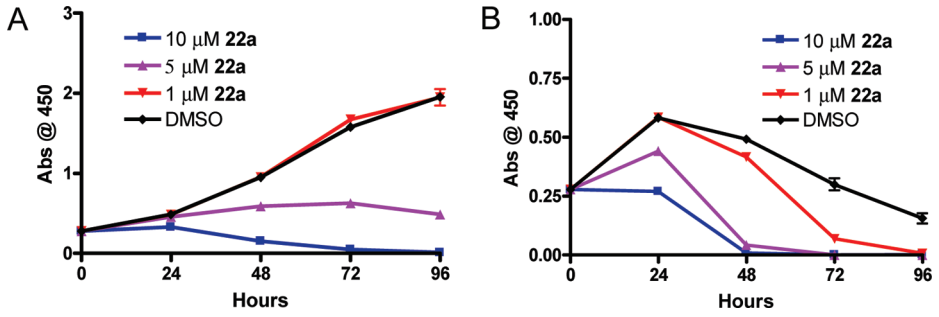

Figure 6. Inhibition of PLD2 leads to a time-dependent decrease in proliferation of MDA-MB-231 cells. MDA-MB-231 cells were cultured in the presence of PLD inhibitor, and cell viability was assayed using WST-1 cell proliferation reagent over 96 h. (A) MDA-MB-231 cells cultured in the presence of 10% FBS showed a dose-dependent attenuation of cell proliferation over time. Cultures with 10 and 5 μM **22a** treatment led to a significant decrease in cell proliferation while 1 μM inhibitor had no effect. (B) MDA-MB-231 cells cultured in the absence of serum had a more pronounced response to PLD inhibition with all concentrations of the PLD2-selective compound significantly decreasing cell proliferation in a dose- and time-dependent manner. Data are representative of three independent experiments. Error bars show standard error of the mean for triplicate measurements.

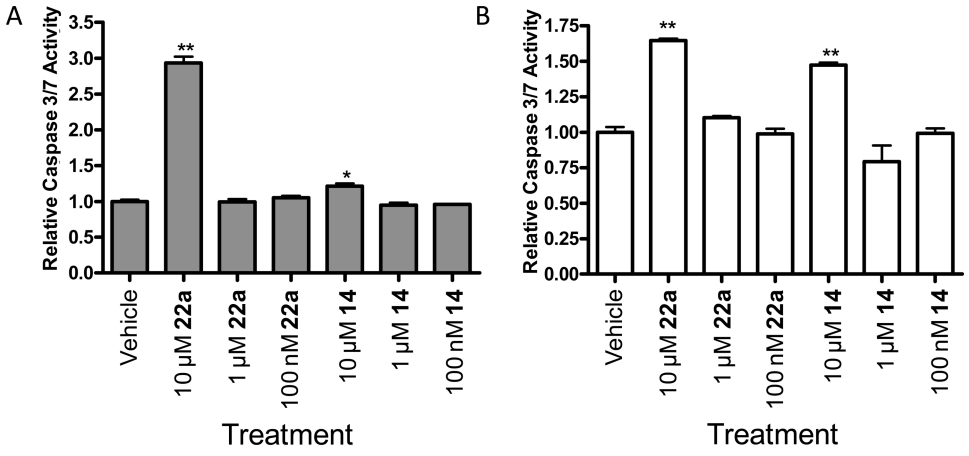

Figure 7. Inhibition of PLD2 leads to increased apoptosis in MDA-MB-231 cells compared with minimal effect of PLD1 inhibition. MDA-MB-231 cells were cultured in the presence of PLD inhibitor for 48 h after which time Caspase 3 and 7 activity was measured. (A) MDA-MB-231 cells cultured in the presence of 10% FBS were fairly resistant to PLD inhibitor treatment (**14** or **22a**) with only 10 μM **22a** treatment leading to a significant increase in Caspase 3 and 7 activity compared to vehicle control. (B) MDA-MB-231 cells cultured under serum-free conditions had increased Caspase 3 and 7 activity upon 10 μM PLD inhibitor treatment as compared to the vehicle control. *, $p < 0.05$; **, $p < 0.01$. Data are representative of three independent experiments. Error bars show standard error of the mean for triplicate measurements.

samples or those cells cultured in the presence of 10% FBS. There are several possible explanations for this observation. These data may suggest that when these cells undergo the stress of serum depravation, survival pathways in which PLD is a key component become essential for cell proliferation, and the inhibition of the PLD enzymatic activity causes a decrease in cell proliferation. Alternatively, the pharmacokinetic properties, specifically plasma protein binding, of these small molecules have not been optimized, and it is likely that a significant percentage of the compound in experiments containing 10% FBS will be serum protein bound. We then evaluated the effect of **22a** on cell proliferation in MDA-MB-231 cells over a 96 h time course and with a dose−response paradigm (Figure 6). In the presence of 10% FBS, **22a** displayed a dose-dependent decrease in cell proliferation over the time course, with significant effects at both a 5 μM and 10 μM dose (Figure 6A). Under serum-free conditions (Figure 6B), a more pronounced effect was observed in a dose- (1, 5, and 10 μM) and time-dependent manner, again suggesting that PLD may be playing a role in the stress response of these cells. Importantly, **22a** was significantly less cytotoxic in standard cell viability assays in nontransformed cells (data not shown).

Next, we evaluated the role of PLD1 and PLD2 inhibition on apoptosis in MDA-MB-231 with and without serum, employing Caspase 3 and 7 activity as a surrogate marker for apoptosis (Figure 7). Once again, our isoform-selective inhibitors were able to distinguish differential roles for PLD1 and PLD2. In the standard 48 h apoptosis assay, a 10 μM dose of PLD2 inhibitor **22a** provided a significant (3-fold increase) increase in Caspase 3 and 7 activity, whereas inhibition of PLD1 with **14** led to a marginal increase in Caspase 3 and 7 activity (Figure 7A). Under serum-free conditions, both **14** and **22a** had similar effects on Caspase 3 and 7 activity (Figure 7B). These data again suggest that PLD2 signaling plays a critical role in the invasive migration, proliferation, and survival of MDA-MB-231 breast cancer cells. Moreover, these data were only obtainable once isoform-selective small molecule PLD1 and PLD2 inhibitors were developed.

Compounds **14** and **22a** were then subjected to a battery of DMPK assays to elucidate their respective disposition characteristics, ultimately in an effort to frame these isoform-selective PLD inhibitors as suitable candidates as in vivo probes of PLD function. PLD1 inhibitor **14** was lipophilic (c log $P = 4.5$) and yet was ~2% free in rat and human plasma protein binding experiments (equilibrium dialysis) with a corresponding ease of

Table 2. Pharmacokinetic Profile of **14** and **22a** in Rat

		iv (pharmacokinetics)[a]				po (plasma and brain levels)[b]			
compd	plasma protein binding (% bound)	dose (mg/kg)	CL (mL min^{-1} kg^{-1})	$t_{1/2}$ (h)	Vd_{ss} (L/kg)	dose (mg/kg)	plasma (ng/mL)	brain (ng/mL)	brain/plasma
14	98.1	1	60.7	0.78	4.7	10	29	BLQ	BLQ
22a	97.9	1	61.5	1.52	8.1	10	39.9	29	0.73

[a] 20% DMSO/80% saline. [b] 10% Tween 80/0.5% methylcellulose.

Scheme 3[a]

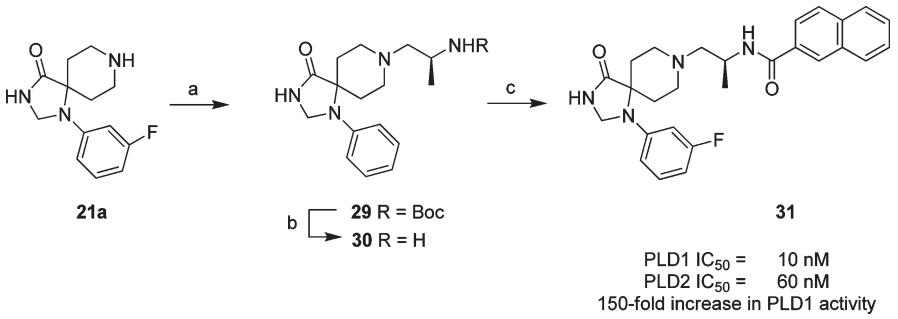

[a] Reagents and conditions: (a) (*S*)-*tert*-butyl 1-oxopropan-2-ylcarbamate, MP-B(OAc)$_3$H, DCM, MeOH, 18 h, 34%; (b) 4.0 M HCl/dioxane, DCM, MeOH, 4 h, 98%; (c) 2-naphthoyl chloride, DIEA, DMF, room temperature, 4 h, 9%.

formulation into dose vehicles amenable to iv and po administration. Parenteral administration to rats (n = 2) revealed **14** to be a highly cleared compound (CL = 60 mL min^{-1} kg^{-1}), approaching that of hepatic blood flow (Q_h) in the rat (Table 2). A corresponding volume of distribution at steady state (Vd_{ss}) for **14** of 4.7 L/kg produced a mean residence time (MRT) of 1.1 h and an effective half-life ($t_{1/2}$) of 0.78 h in rat. A similar profile was obtained for PLD2 inhibitor **22a**. While less lipophilic (*c* log P = 3.2), **22a** also displayed ~2% free fraction in rat and human plasma protein binding experiments (equilibrium dialysis) and was easily formulated into acceptable vehicles. Similarly, parenteral administration to rats revealed **22a** to be a highly cleared compound (CL = 61 mL min^{-1} kg^{-1}), with a high volume of distribution (Vd_{ss} = 8.1 L/kg), a 2.2 h MRT, and a corresponding effective $t_{1/2}$ of 1.5 h. Employing rat hepatic microsomes, the intrinsic clearance values (CL_{int}, eqs 1 and 2) for **14** and **22a** were determined to be 660 and 203 mL min^{-1} kg^{-1}, respectively (data not shown), and converted to predicted hepatic clearance (CL_{hep}), utilizing the well-stirred model of hepatic clearance (eq 3), produced CL_{hep} values of 63 and 52 mL min^{-1} kg^{-1}. The general agreement between in vitro and in vivo clearance (CL and CL_{hep}) values indicate hepatic metabolism to be a likely mechanism contributing to the disposition of **14** and **22a**.

Recent genetic and knockout studies have suggested therapeutic roles for PLD inhibition in Alzheimer's disease[29,30] and stroke;[31] therefore, PLD inhibitors with exceptional CNS bioavailability would be of great value for preclinical target validation. To address CNS penetration, fasted Sprague-Dawley rats (n = 2) received a single, oral gavage of **14** and **22a** at a dose of 10 mg/kg in a typical 90 min single point brain:plasma (PBL) study design. While levels of **14** were below quantitation in the brain, the napthylene analogue **22a** displayed a brain:plasma value of 0.73, thereby representing the first centrally penetrant PLD inhibitor. While **14** and **22a** remain important in vitro tools to probe and describe the differential roles and pharmacology of PLD1 and PLD2, additional optimization will be required to develop robust in vivo proof-of-concept compounds. These data also suggest

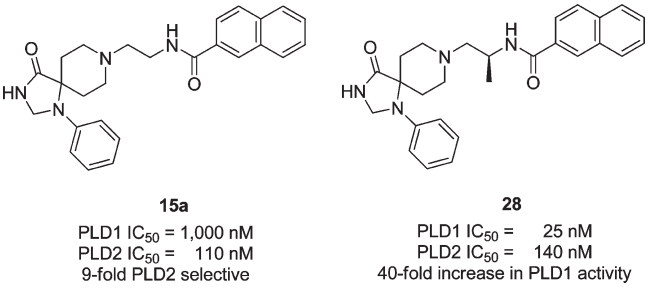

Figure 8. Structures and activities of PLD2-preferring inhibitor **15a** and impact of a chiral (*S*)-methyl group providing **28** and a 40-fold increase in PLD inhibitory activity.

that the differences observed in the cellular experiments involving the presence and absence of serum could be due to the lipophillic character of these compounds and the result that ~2% is displayed as free fraction in rat and human plasma protein binding experiments.

Finally, the impact of incorporating an (*S*)-methyl group was found to be important for increasing PLD inhibitory activity in the PLD1-selective benzimidazolone series represented by **13** and **14**. Installation of the (*S*)-methyl group into the modestly PLD2-preferring **15a** (PLD1 IC_{50} = 1000 nM, PLD2 IC_{50} = 110 nM), within the triazaspirone series (Figure 8), resulted in **28** with enhanced (40-fold) PLD1 inhibition and essentially no effect on PLD2 activity (PLD1 IC_{50} = 25 nM, PLD2 IC_{50} = 140 nM).[28] This type of "molecular switch" has been noted before for allosteric modulators of GPCRs engendering either subtype selectivity or reversing the mode of pharmacology (NAM to PAM or PAM to NAM). Thus, we wanted to evaluate if the addition of the PLD1-preferring (*S*)-methyl "molecular switch" would increase PLD1 inhibitory activity in a highly PLD2-preferring compound such as **22a**. In the event, **22a** underwent a reductive amination with (*S*)-*tert*-butyl 1-oxopropan-2-ylcarbamate to provide **29**, which was then deprotected to provide **30**. Acylation with 2-naphthoyl chloride afforded the (*S*)-methyl analogues **31** of **22a** (Scheme 3). Evaluation of **31** in our PLD1 and PLD2

cellular assays (Calu-1 and HEK293-gfpPLD2, respectively) further highlighted the impact of the (*S*)-methyl group as a "molecular switch" for these allosteric ligands, providing a 150-fold increase in PLD1 inhibitory activity (PLD2 IC_{50} = 10 nM) while maintaining PLD2 activity (PLD2 IC_{50} = 60 nM). Thus, a 75-fold PLD2-preferring inhibitor **22a** is converted into a potent dual PLD1/2 inhibitor **31** by the addition of a single methyl group.

Conclusion

In summary, we have developed the most potent (PLD2 IC_{50} = 20 nM) and selective (75-fold versus PLD1) PLD2 inhibitor **22a** described. Due to the shallow and unpredictable SAR for these allosteric PLD inhibitors, a matrix library approach enabled the rapid discovery of **22a**, whereas a classical singleton approach probably would have failed to discover **22a**. As with other allosteric ligand optimization programs, SAR proved to be shallow and somewhat unpredictable for the triazaspirone series, with PLD potency and PLD2 selectivity dependent on both the halogen substituent on the triazaspirone scaffold and the nature of the amide moiety. With potent and selective PLD1 and PLD2 inhibitors in hand, we were able to dissect the relative contributions of PLD1 and PLD2 signaling on proliferation and survival of the triple negative breast cancer cell line MDA-MB-231. In all instances, selective PLD2 inhibition with **22a** displayed significant effects and suggests that for this cancer cell line a PLD2 inhibitor, not a PLD1 or a dual PLD1/2 inhibitor, would be the optimal therapeutic agent. Introduction of a "molecular switch", in the form of an (*S*)-methyl group, to **22a** increased PLD1 activity 150-fold, providing a potent PLD1/2 inhibitor **31**. Current efforts are focused on employing **14** and **22a** to dissect the contributions of PLD1 and PLD2 signaling in other cancer cell lines as well as developing additional isoform-selective PLD inhibitors with improved DMPK properties which will enable the discovery of new indications, such as schizophrenia, stroke, and Alzheimer's disease, where aberrant PLD activity is implicated.

Experimental Section

All reactions were carried out employing standard chemical techniques. Unless otherwise noted, reactions were run in anhydrous solvents. Solvents for extraction, washing, and chromatography were HPLC grade. All reagents were purchased from Sigma-Aldrich and Biotage at the highest commercial quality and were used without purification. Microwave-assisted reactions were conducted using a Biotage Initiator-60 single mode microwave synthesizer. All NMR spectra were recorded on a 400 MHz Bruker AMX NMR. ^{1}H chemical shifts are reported as δ values in ppm relative to the solvent residual peak (MeOD = 3.31, DMSO-d_6 = 2.50, $CDCl_3$ = 7.26). Data are reported as follows: chemical shift, multiplicity (s = singlet, d = doublet, t = triplet, q = quartet, m = multiplet), coupling constant (Hz), and integration. ^{13}C chemical shifts are reported as δ values in ppm relative to the solvent residual peak (MeOD = 49.0, DMSO-d_6 = 39.5, $CDCl_3$ = 77.16). Low-resolution mass spectra were obtained on an Agilent 1200 LC-MS with electrospray ionization equipped with a YMC Jsphere H-80 S-4 3.0 × 50 mm column running a gradient of 5%−95% (over 4 min) acetonitrile in 0.1% trifluoroacetic acid in water. Low-resolution mass spectra for compounds **30** and **31** were obtained on an Agilent 1200 LC-MS with electrospray ionization equipped with a Phenomenex Kinetex 2.1 × 50 mm C18 column running a gradient of 10%−95% (over 45 s) acetonitrile in 0.1% trifluoroacetic acid in water. High-resolution mass spectra were recorded on a Waters QToF-API-US plus Acquity system with electrospray ionization. Analytical thin-layer chromatography was performed on 250 μm silica gel 60 F254 plates. Automated flash column chromatography was performed on a Teledyne ISCO combiflash Rf system. Analytical HPLC was performed on an Agilent 1200 analytical LC-MS equipped with a YMC Jsphere H-80 S-4 3.0 × 50 mm column running a gradient of 5%−95% (at a flow rate of 1.25 mL/min over 4 min) acetonitrile in 0.1% trifluoroacetic acid in water and UV detection at 214 and 254 nm along with ELSD detection. Analytical HPLC for compounds **30** and **31** was performed on an Agilent 1200 LC-MS with electrospray ionization equipped with a Phenomenex Kinetex 2.1 × 50 mm C18 column running a gradient of 10%−95% (over 45 s) acetonitrile in 0.1% trifluoroacetic acid in water and UV detection at 214 and 254 nm. Preparative purification of library compounds was performed on a custom Agilent 1200 preparative LC-MS with collection triggered by mass detection, or alternatively compounds were purified on a Gilson 215 preparative LC system equipped with a Phenomenx Luna 5u C18 50×30 mm column by running a gradient of 20%−60% acetonitrile in 0.1% trifluoroacetic acid in water at a flow rate of 50 mL/min over approximately 5 min. All compounds described within this report are >95% pure by HPLC (254 nm, 214 nm, and ELSD) as well as ^{1}H NMR. All yields refer to analytically pure and fully characterized materials (^{1}H NMR, ^{13}C NMR, analytical LC-MS, and HRMS).

1-Benzyl-4-((3-fluorophenyl)amino)piperidine-4-carboxamide (18a). To a solution of 1-benzylpiperidin-4-one (13.25 g, 70 mmol) in glacial acetic acid (70 mL) and water (12 mL) cooled to 0 °C were added 3-fluoroaniline (8.55 g, 77 mmol) and potassium cyanide (4.55 g, 70 mmol). The reaction was allowed to warm to room temperature and agitated for approximately 12 h. The reaction was then cooled to 0 °C, and ammonium hydroxide (18 M) was added dropwise until the solution pH was 11 or greater. The mixture was then extracted into dichloromethane and dried under reduced pressure to yield the crude product as a tan oil (20.5 g). The crude product was then immediately cooled to 0 °C, and concentrated sulfuric acid (18 M, 120 mL) was added dropwise. The reaction was allowed to warm to room temperature and agitated for approximately 12 h. The reaction was then cooled to 0 °C, and ammonium hydroxide (18 M) was added dropwise until the solution pH was 11 or greater. The mixture was then extracted into dichloromethane and dried under reduced pressure to afford a tan solid (15.78 g, 48.25 mmol, 68%). ^{1}H NMR (400.1 MHz, $CDCl_3$) δ (ppm): 7.51−7.37 (m, 7H), 6.67−6.47 (m, 4H), 4.27 (s, 1H), 3.64 (s, 2H), 2.95−2.87 (m, 2H), 2.53−2.44 (m, 2H), 2.29−2.21 (m, 2H), 2.07 (d, J = 13 Hz, 2H). ^{13}C NMR (100.6 MHz, $CDCl_3$) δ (ppm): 178.0, 162.6, 145.7, 138.3, 130.5, 129.1 (2C), 128.4 (2C), 127.2, 111.8, 106.1, 103.1, 63.1, 58.5, 48.7 (2C), 34.8, 31.5. HRMS (TOF, ESI) $C_{19}H_{23}N_3OF$ $[M + H]^+$ calculated 328.1825, found 328.1827. LC-MS: rt (min) = 1.855. LRMS (ESI) m/z = 328.2.

1-(3-Fluorophenyl)-1,3,8-triazaspiro[4.5]decan-4-one (20a). 1-Benzyl-4-((3-fluorophenyl)amino)piperidine-4-carboxamide **18a** (15.78 g, 48.25 mmol), trimethyl orthoformate (80 mL), and glacial acetic acid (40 mL) were combined and subjected to microwave irradiation at 150 °C for 15 min. The mixture was adjusted to pH 12 with ammonium hydroxide (18 M) and extracted into dichloromethane and dried under reduced pressure. This material was then added to a suspension of sodium borohydride (4.56 g, 120.6 mmol) in methanol (150 mL) and stirred for about 3 h. The reaction was quenched with water, extracted into dichloromethane, and dried under reduced pressure. The material was then chromatographed on a 330 g flash column (Teledyne) as follows: (1) a gradient from 0% to 80% ethyl acetated in hexanes over 10 min was run, and on the same column (2) a gradient from 0% to 10% methanol in dichloromethane was run. The purity of the isolated intermediate compound was established via LC-MS: rt (min) 1.723; LRMS (ESI) m/z = 340.1. This intermediate **19a** (1.94 g) was immediately

dissolved in methanol (40 mL) and glacial acetic acid (10 mL) and treated with palladium on carbon (cat., 80 mg) under an atmosphere of hydrogen. After about 36 h the reaction mixture was filtered through Celite, concentrated under reduced pressure, diluted with water, made alkaline with saturated sodium bicarbonate, and extracted 8 times into dichloromethane to afford a white solid (1.37 g, 5.49 mmol, 11%). ^{1}H NMR (400.1 MHz, DMSO-d_6) δ (ppm): 8.67 (s, 1H), 7.20 (q, J = 8 Hz, 1H), 6.73 (d, J = 8 Hz, 1H), 6.62 (d, J = 13 Hz, 1H), 6.52−6.46 (m, 1H), 4.57 (s, 2H), 3.20−3.09 (m, 3H), 2.91−2.82 (m, 2H), 2.46−2.36 (m, 2H), 1.48 (d, J = 14 Hz, 2H). ^{13}C NMR (100.6 MHz, DMSO-d_6) δ (ppm): 176.0, 164.3, 145.0, 130.1, 109.3, 103.1, 100.2, 58.8, 58.6, 42.1 (2C), 28.9 (2C). HRMS (TOF, ESI) $C_{13}H_{17}N_3OF$ [M + H]$^+$ calculated 250.1356, found 250.1351. LC-MS: rt (min) = 1.394. LRMS (ESI) m/z = 250.1.

8-(2-Aminoethyl)-1-(3-fluorophenyl)-1,3,8-triazaspiro[4.5]decan-4-one Dihydrochloride (21a). 1-(3-Fluorophenyl)-1,3,8-triazaspiro[4.5]decan-4-one **20a** (1370 mg, 5.49 mmol) and *tert*-butyl (2-oxoethyl)carbamate (961 mg, 6.03 mmol) were combined and dissolved in dichloromethane (25 mL) and methanol (10 mL) and stirred for about 30 min at room temperature. After about 30 min macroporous triacetoxyborohydride (3 g, 7.26 mmol) was added to the reaction, and after 14 h an additional amount of *tert*-butyl (2-oxoethyl)carbamate (200 mg, 1.25 mmol) was added to drive the reaction to completion. After about 24 h the reaction mixture was filtered through Celite and concentrated under reduced pressure. The crude compound was chromatographed on an 80 g flash column eluting in a gradient of 0%−10% methanol in dichloromethane to afford a white solid (1.64 g, 4.18 mmol, 76%). ^{1}H NMR (400.1 MHz, DMSO-d_6) δ (ppm): 8.69 (s, 1H), 7.22 (q, J = 8 Hz, 1H), 6.72−6.63 (m, 2H), 6.60−6.49 (m, 2H), 4.58 (s, 2H), 2.83−2.75 (m, 2H), 2.74−2.65 (m, 2H), 2.61−2.48 (m, 2H), 2.42−2.35 (m, 2H), 1.91 (s, 2H), 1.55 (d, J = 13 Hz, 2H), 1.39 (s, 9H). ^{13}C NMR (100.6 MHz, DMSO-d_6) δ (ppm): 175.8, 161.9, 155.6, 145.0, 130.4, 109.4, 103.2, 100.3, 77.5, 58.7, 58.1, 57.4, 49.3 (2C), 37.6, 28.3 (3C), 28.1 (2C). HRMS (TOF, ESI) $C_{20}H_{30}N_4O_3F$ [M + H]$^+$ calculated 393.2302, found 393.2301. LC-MS: rt (min) = 1.966. LRMS (ESI) m/z = 393.2. *tert*-Butyl (2-(1-(3-fluorophenyl)-4-oxo-1,3,8-triazaspiro[4.5]decan-8-yl)ethyl)carbamate (1.64 g, 4.18 mmol) was dissolved in dichloromethane (40 mL) and a minimal amount of methanol added dropwise. Hydrochloric acid was added (4 M in dioxane, 20 mL), and the reaction was stirred for approximately 36 h at room temperature. The reaction was concentrated under reduced pressure to afford a white solid (1.34 g, 3.66 mmol, 88%). ^{1}H NMR (400.1 MHz, DMSO-d_6) δ (ppm): 9.12 (s, 1H), 8.47 (s, 2H), 7.18 (q, J = 8 Hz, 1H), 7.07−7.02 (m, 1H), 6.79−6.72 (m, 1H), 6.57−6.50 (m, 1H), 4.63 (s, 2H), 3.72−3.56 (m, 4H), 3.45−3.38 (m, 4H), 3.10−3.00 (m, 2H), 1.90 (d, J = 15 Hz, 2H), ^{13}C NMR (100.6 MHz, DMSO-d_6) δ (ppm): 174.4, 162.3, 144.4, 130.3, 109.8, 103.8, 100.2, 69.0, 56.5, 53.3, 49.1 (2C), 33.8, 25.6 (2C). HRMS (TOF, ESI) $C_{15}H_{22}N_4OF$ [M + H]$^+$ calculated 293.1778, found 293.1776. LC-MS: rt (min) = 1.405. LRMS (ESI) m/z = 293.1.

***N*-(2-(1-(3-Fluorophenyl)-4-oxo-1,3,8-triazaspiro[4.5]decan-8-yl)ethyl)-2-naphthamide (22a).** 8-(2-Aminoethyl)-1-(3-fluorophenyl)-1,3,8-triazaspiro[4.5]decan-4-one dihydrochloride **21a** (1.23 g, 3.37 mmol), 2-naphthoyl chloride (641 mg, 3.37 mmol), and *N*,*N*-diisopropylethylamine (2.05 mL, 11.7 mmol) were all dissolved in *N*,*N*-dimethylformamide (20 mL) at 0 °C. The reaction mixture was allowed to warm to room temperature and stirred for about 12 h. The reaction mixture was diluted with water and extracted into dichloromethane 5 times. The dichloromethane layer was then washed 3 times with a solution of lithium chloride (3 M) and dried under reduced pressure. The reaction mixture was chromatographed on an 80 g flash column eluting in 0%−5% methanol in dichloromethane to afford a white solid (1.25 g, 2.80 mmol, 83%). ^{1}H NMR (400.1 MHz, DMSO-d_6) δ (ppm): 8.69 (s, 1H), 8.60 (t, J = 5 Hz, 1H), 8.45 (s, 1H), 8.04−7.92 (m, 4H), 7.64−7.56 (m, 2H), 7.11 (q, J = 8 Hz, 1H), 6.68−6.63 (m, 1H), 6.58−6.52 (m, 1H), 6.49−6.43 (m, 1H), 4.58 (s, 2H), 3.48 (q, J = 6 Hz, 2H), 2.91−2.83 (m, 2H), 2.80−2.72 (m, 2H), 2.64−2.53 (m, 4H), 1.58 (d, J = 14 Hz, 2H). ^{13}C NMR (100.6 MHz, DMSO-d_6) δ (ppm): 175.9, 166.2, 164.3, 161.9, 145.0, 134.1, 132.2, 130.3, 128.8, 127.8, 127.6, 127.5, 127.3, 126.7, 124.1, 109.3, 103.3, 100.3, 58.7, 58.1, 56.9, 49.4 (2C), 37.3, 28.2 (2C). HRMS (TOF, ESI) $C_{26}H_{28}N_4O_2F$ [M + H]$^+$ calculated 447.2196, found 447.2195. LC-MS: rt (min) = 2.287. LRMS (ESI) m/z = 447.2. Analogues **22b−d** were made following the same protocol starting from **21a** and were purified via reversed-phase chromatography to greater than 95% purity (as trifluoroacetate salts) as analyzed by ELSD and UV at both 214 and 254 nM.

***N*-(2-(1-(3-Fluorophenyl)-4-oxo-1,3,8-triazaspiro[4.5]decan-8-yl)ethyl)-2-naphthamide Hydrochloride (22a·HCl).** *N*-(2-(1-(3-Fluorophenyl)-4-oxo-1,3,8-triazaspiro[4.5]decan-8-yl)ethyl)-2-naphthamide **22a** (1.25 mg, 2.80 mmol) was stirred in methanol (30 mL) at room temperature and treated with hydrochloric acid (4 M in dioxane, 4 mL). After about 25 min the compound was dried under reduced pressure to afford a white solid (1.31 g, 2.72 mmol, 97%). ^{1}H NMR (400.1 MHz, DMSO-d_6) δ (ppm): 10.99 (s, 1H), 9.14 (t, J = 5 Hz, 1H), 9.11 (s, 1H), 8.60 (s, 1H), 8.06−7.97 (m, 4H), 7.65−7.57 (m, 2H), 7.21 (q, J = 8 Hz, 1H), 7.05−7.01 (m, 1H), 6.83−6.77 (m, 1H), 6.58−6.52 (m, 1H), 4.64 (s, 2H), 3.85−3.75 (m, 2H), 3.74−3.64 (m, 4H), 3.41−3.36 (m, 2H), 3.11−2.99 (m, 2H), 1.92 (d, J = 14 Hz, 2H). ^{13}C NMR (100.6 MHz, DMSO-d_6) δ (ppm): 174.4, 166.6, 164.6, 162.2, 144.6, 134.3, 132.1, 131.2, 130.5, 128.9, 127.9, 127.8, 127.6, 126.8, 124.2, 109.9, 104.0, 100.3, 59.0, 56.6, 55.7, 48.7 (2C), 34.4, 25.7 (2C). HRMS (TOF, ESI) $C_{26}H_{28}N_4O_2F$ [M + H]$^+$ calculated 447.2196, found 447.2186. LC-MS: rt (min) = 2.264. LRMS (ESI) m/z = 447.2.

8-(2-Aminoethyl)-1-(3-chlorophenyl)-1,3,8-triazaspiro[4.5]decan-4-one Dihydrochloride (21b). 1-(3-Chlorophenyl)-1,3,8-triazaspiro[4.5]decan-4-one **20b** (127 mg, 0.47 mmol) and *tert*-butyl (2-oxoethyl)carbamate (83.8 mg, 0.51 mmol) were combined and dissolved in dichloromethane (1.5 mL) and methanol (0.05 mL) and stirred for about 30 min at room temperature. After about 30 min macroporous triacetoxyborohydride (600 mg, 1.4 mmol) was added to the reaction, and after 14 h an additional amount of *tert*-butyl (2-oxoethyl)carbamate (41.9 mg, 0.25 mmol) was added to drive the reaction to completion. After about 24 h the reaction mixture was filtered through Celite and concentrated under reduced pressure. The crude compound was chromatographed on a 12 g flash column eluting in a gradient of 0%−10% methanol in dichloromethane to afford a white solid (72 mg, 0.18 mmol, 37%). ^{1}H NMR (400.1 MHz, MeOD) δ (ppm): 7.21 (t, J = 9 Hz, 1H), 6.95−6.90 (m, 2H), 6.86−6.78 (m, 1H), 4.69 (s, 2H), 3.23−3.02 (m, 4H), 2.81−2.67 (m, 4H), 1.97 (s, 2H), 1.78 (d, J = 14 Hz, 2H), 1.45 (s, 9H). ^{13}C NMR (100.6 MHz, MeOD) δ (ppm): 178.2, 158.5, 145.8, 136.2, 141.3, 119.5, 115.4, 114.2, 80.3, 60.4, 60.1, 58.4, 50.7 (2C), 38.1, 29.2 (2C). 28.7 (3C). HRMS (TOF, ESI) $C_{20}H_{30}N_4O_3Cl$ [M + H]$^+$ calculated 409.2006, found 409.1996. LC-MS: rt (min) = 1.984. LRMS (ESI) m/z = 409.2. *tert*-Butyl (2-(1-(3-chlorophenyl)-4-oxo-1,3,8-triazaspiro[4.5]decan-8-yl)ethyl)carbamate (72 mg, 0.17 mmol) was dissolved in dichloromethane (5 mL) and a minimal amount of methanol added dropwise. Hydrochloric acid was added (4 M in dioxane, 1.0 mL), and the reaction was stirred for approximately 16 h at room temperature. The reaction was concentrated under reduced pressure to afford a white solid (60 mg, 0.16 mmol, 93%). ^{1}H NMR (400.1 MHz, MeOD) δ (ppm): 7.25 (t, J = 8 Hz, 1H), 7.20−7.15 (m, 1H), 6.88−6.81 (m, 2H), 4.74 (s, 2H), 3.96−3.86 (m, 2H), 3.73−3.65 (m, 2H), 3.51 (s, 4H), 3.20−3.10 (m, 2H), 2.05 (d, J = 15 Hz, 2H). ^{13}C NMR (100.6 MHz, MeOD) δ (ppm): 176.9, 145.2, 135.6, 131.5, 119.9, 115.1, 114.4, 60.5, 58.4, 54.9, 51.2 (2C), 35.4, 27.8 (2C). HRMS (TOF, ESI) $C_{15}H_{22}N_4OCl$ [M + H]$^+$ calculated

309.1482, found 308.1480. LC-MS: rt (min) = 1.413. LRMS (ESI) m/z = 309.1.

***N*-(2-(1-(3-Chlorophenyl)-4-oxo-1,3,8-triazaspiro[4.5]decan-8-yl)-ethyl)-2-naphthamide 2,2,2-Trifluoroacetate (23a).** 8-(2-Aminoethyl)-1-(3-chlorophenyl)-1,3,8-triazaspiro[4.5]decan-4-one dihydrochloride **21b** (60 mg, 0.15 mmol), 2-naphthoyl chloride (30.0 mg, 0.15 mmol), and *N*,*N*-diisopropylethylamine (0.115 mL, 0.66 mmol) were all dissolved in *N*,*N*-dimethylformamide (1 mL) at 0 °C. The reaction mixture was allowed to warm to room temperature and stirred for about 12 h. The reaction mixture was diluted with water and extracted into dichloromethane 5 times. The dichloromethane layer was then washed 3 times with a solution of lithium chloride (3 M) and dried under reduced pressure. The reaction mixture was subjected to reversed-phase chromatography to afford a white solid (43.4 mg, 0.075 mmol, 50%). ^{1}H NMR (400.1 MHz, DMSO-d_6) δ (ppm): 9.32 (s, 1H), 9.13 (s, 1H), 9.01 (t, J = 5 Hz, 1H), 8.50 (s, 1H), 8.06−7.94 (m, 4H), 7.66−7.58 (m, 2H), 7.22 (t, J = 8 Hz, 1H), 6.98−6.94 (m, 1H), 6.86−6.80 (m, 2H), 4.65 (s, 2H), 3.79−3.68 (m, 6H), 3.44−3.39 (m, 2H), 2.88−2.75 (m, 2H), 1.97 (d, J = 15 Hz, 2H). ^{13}C NMR (100.6 MHz, DMSO-d_6) δ (ppm): 174.3, 167.0, 158.6, 144.2, 134.3, 134.2, 132.1, 131.2, 130.4, 128.9 (2C), 128.0, 127.8, 127.7 (2C), 126.9, 124.1, 117.7, 113.2, 112.5, 59.0, 56.6, 55.3, 48.9 (2C), 34.6, 26.0 (2C). HRMS (TOF, ESI) $C_{26}H_{28}N_4O_2Cl$ $[M + H]^+$ calculated 463.1901, found 463.1894. LC-MS: rt (min) = 2.266. LRMS (ESI) m/z = 463.1. Analogues **23b−d** were made following the same protocol starting from **21b** and were purified via reversed-phase chromatography to greater than 95% purity (as trifluoroacetate salts) as analyzed by ELSD and UV at both 214 and 254 nM.

(*S*)-8-(2-Aminopropyl)-1-(3,4-difluorophenyl)-1,3,8-triazaspiro-[4.5]decan-4-one Dihydrochloride (21c). 1-(3,4-Difluorophenyl)-1,3,8-triazaspiro[4.5]decan-4-one **20c** (104.8 mg, 0.39 mmol) and (*S*)-*tert*-butyl (1-oxopropan-2-yl)carbamate (74.6 mg, 0.43 mmol) were combined and dissolved in dichloromethane (1.5 mL) and methanol (0.05 mL) and stirred for about 30 min at room temperature. After about 30 min macroporous triacetoxyborohydride (600 mg, 1.4 mmol) was added to the reaction, and after 14 h an additional amount of (*S*)-*tert*-butyl (1-oxopropan-2-yl)carbamate (37.3 mg, 0.22 mmol) was added to drive the reaction to completion. After about 24 h the reaction mixture was filtered through Celite and concentrated under reduced pressure. The crude compound was chromatographed on a 12 g flash column eluting in a gradient of 0%−10% methanol in dichloromethane to afford a white solid (60 mg, 0.14 mmol, 36%). ^{1}H NMR (400.1 MHz, MeOD) δ (ppm): 7.15 (q, J = 10 Hz, 1H), 7.00−6.92 (m, 1H), 6.76−6.70 (m, 1H), 4.67 (s, 2H), 3.98−3.80 (m, 1H), 3.18−3.09 (m, 1H), 2.83−2.52 (m, 5H), 1.96 (s, 2H), 1.83 (d, J = 14 Hz, 2H), 1.45 (s, 9H), 1.17 (d, J = 7 Hz, 3H). ^{13}C NMR (100.6 MHz, MeOD) δ (ppm): 178.0, 158.1, 152.9, 150.6, 141.5, 118.4, 113.2, 106.3, 80.5, 63.8, 60.8, 59.9, 51.4 (2C), 44.6, 29.1 (2C), 28.7 (3C), 19.6. HRMS (TOF, ESI) $C_{21}H_{31}N_4O_3F_2$ $[M + H]^+$ calculated 425.2364, found 425.2367. LC-MS: rt (min) = 2.028. LRMS (ESI) m/z = 425.2. (*S*)-*tert*-Butyl (1-(1-(3,4-difluorophenyl)-4-oxo-1,3,8-triazaspiro[4.5]decan-8-yl)propan-2-yl)carbamate (60 mg, 0.14 mmol) was dissolved in dichloromethane (5 mL) and a minimal amount of methanol added dropwise. Hydrochloric acid was added (4 M in dioxane, 1.0 mL), and the reaction was stirred for approximately 16 h at room temperature. The reaction was concentrated under reduced pressure to afford a white solid (51 mg, 0.13 mmol, 93%). ^{1}H NMR (400.1 MHz, DMSO-d_6) δ (ppm): 9.12 (s, 1H), 8.61 (br s, 2H), 7.18 (q, J = 9 Hz, 1H), 7.12−7.05 (m, 1H), 7.01−6.95 (m, 1H), 4.60 (s, 2H), 3.96−3.57 (m, 5H), 3.56−3.46 (m, 2H), 3.06−2.92 (m, 2H), 1.91 (d, J = 15 Hz, 2H), 1.32 (d, J = 7 Hz, 3H). ^{13}C NMR (100.6 MHz, DMSO-d_6) δ (ppm): 174.4, 151.2, 148.8, 139.9, 117.2, 110.2, 103.2, 59.4, 59.2, 56.6, 50.6, 48.6, 42.5, 25.8, 25.6, 17.1. HRMS (TOF, ESI) $C_{16}H_{23}N_4OF_2$ $[M + H]^+$ calculated 325.1840, found 325.1839. LC-MS: rt (min) = 1.344. LRMS (ESI) m/z = 325.1.

(*S*)-*N*-(1-(1-(3,4-Difluorophenyl)-4-oxo-1,3,8-triazaspiro[4.5]-decan-8-yl)propan-2-yl)-2-naphthamide 2,2,2-Trifluoroacetate (24a). (*S*)-8-(2-Aminopropyl)-1-(3,4-difluorophenyl)-1,3,8-triazaspiro-[4.5]decan-4-one dihydrochloride **21c** (40 mg, 0.10 mmol), 2-naphthoyl chloride (19.1 mg, 0.10 mmol), and *N*,*N*-diisopropylethylamine (0.073 mL, 0.42 mmol) were all dissolved in *N*,*N*-dimethylformamide (1 mL) at 0 °C. The reaction mixture was allowed to warm to room temperature and stirred for about 12 h. The reaction mixture was diluted with water and extracted into dichloromethane 5 times. The dichloromethane layer was then washed 3 times with a solution of lithium chloride (3 M) and dried under reduced pressure. The reaction mixture was subjected to reversed-phase chromatography to afford a white solid (29.2 mg, 0.05 mmol, 49%). ^{1}H NMR (400.1 MHz, DMSO-d_6) δ (ppm): 9.69 (s, 1H), 9.08 (s, 1H), 8.77 (d, J = 8 Hz, 1H), 8.50 (s, 1H), 8.05−7.95 (m, 4H), 7.66−7.58 (m, 2H), 7.25 (q, J = 10 Hz, 1H), 7.02−6.95 (m, 1H), 6.74−6.69 (m, 1H), 4.59 (s, 2H), 3.85−3.68 (m, 4H), 3.60−3.53 (m, 1H), 3.43−3.31 (m, 2H), 2.78−2.57 (m, 2H), 2.01−1.89 (m, 2H), 1.31 (d, J = 7 Hz, 3H). ^{13}C NMR (100.6 MHz, DMSO-d_6) δ (ppm): 174.3, 166.5, 158.2, 148.6, 140.1, 134.3, 132.1, 131.4, 128.8, 127.8, 127.7 (2C), 127.6, 126.8, 124.4, 117.6, 117.5, 110.9, 104.1, 103.9, 60.7, 59.2, 56.7, 49.8, 48.6, 41.2, 26.1, 26.0, 19.0. HRMS (TOF, ESI) $C_{27}H_{29}N_4O_2F_2$ $[M + H]^+$ calculated 479.2259, found 479.2262. LC-MS: rt (min) = 2.286. LRMS (ESI) m/z = 479.2. Analogues **24b−d** were made following the same protocol starting from **21c** and were purified via reversed-phase chromatography to greater than 95% purity (as trifluoroacetate salts) as analyzed by ELSD and UV at both 214 and 254 nM.

8-(2-Aminoethyl)-1-(4-fluorophenyl)-1,3,8-triazaspiro[4.5]-decan-4-one Dihydrochloride (21d). 1-(4-Fluorophenyl)-1,3,8-triazaspiro[4.5]decan-4-one **20d** (54.8 mg, 0.22 mmol) and *tert*-butyl (2-oxoethyl)carbamate (38.2 mg, 0.24 mmol) were combined and dissolved in dichloromethane (1.5 mL) and methanol (0.05 mL) and stirred for about 30 min at room temperature. After about 30 min macroporous triacetoxyborohydride (600 mg, 1.4 mmol) was added to the reaction, and after 14 h an additional amount of *tert*-butyl (2-oxoethyl)carbamate (19.1 mg, 0.12 mmol) was added to drive the reaction to completion. After about 24 h the reaction mixture was filtered through Celite and concentrated under reduced pressure. The crude compound was chromatographed on a 12 g flash column eluting in a gradient of 0%−10% methanol in dichloromethane to afford a white solid (41 mg, 0.10 mmol, 47%). ^{1}H NMR (400.1 MHz, MeOD) δ (ppm): 7.10−7.02 (m, 4H), 4.67 (s, 2H), 3.28−3.24 (m, 2H), 3.20−3.12 (m, 2H) 2.86−2.80 (m, 2H), 2.44−2.37 (m, 2H), 1.95 (s, 2H), 1.88 (d, J = 14 Hz, 2H), 1.44 (s, 9H). ^{13}C NMR (100.6 MHz, MeOD) δ (ppm): 178.4, 160.7, 158.4, 140.8, 122.3, 122.2, 116.7, 116.5, 80.4, 61.2, 60.1, 58.1, 50.6 (2C), 37.5, 29.5 (2C), 28.7 (3C). HRMS (TOF, ESI) $C_{20}H_{30}N_4O_3F$ $[M + H]^+$ calculated 393.2302, found 393.2300. LC-MS: rt (min) = 1.850. LRMS (ESI) m/z = 393.2. *tert*-Butyl (2-(1-(4-fluorophenyl)-4-oxo-1,3,8-triazaspiro[4.5]decan-8-yl)ethyl)carbamate (41 mg, 0.10 mmol) was dissolved in dichloromethane (5 mL) and a minimal amount of methanol added dropwise. Hydrochloric acid was added (4 M in dioxane, 0.5 mL), and the reaction was stirred for approximately 16 h at room temperature. The reaction was concentrated under reduced pressure to afford a white solid (34 mg, 0.093 mmol, 93%). ^{1}H NMR (400.1 MHz, MeOD) δ (ppm): 7.16−7.08 (m, 2H), 7.08−7.00 (m, 2H), 4.72 (s, 2H), 3.92−3.81 (m, 2H), 3.72−3.63 (m, 2H), 3.50 (s, 4H), 2.93−2.81 (m, 2H), 2.05 (d, J = 15 Hz, 2H). ^{13}C NMR (100.6 MHz, MeOD) δ (ppm): 177.3, 160.3, 140.1, 120.5, 120.4, 116.9, 116.7, 61.1, 58.6, 54.9, 51.3 (2C), 35.4, 28.5 (2C). HRMS (TOF, ESI) $C_{15}H_{22}N_4OF$ $[M + H]^+$ calculated 293.1778, found 293.1769. LC-MS: rt (min) = 1.260. LRMS (ESI) m/z = 293.2.

***N*-(2-(1-(4-Fluorophenyl)-4-oxo-1,3,8-triazaspiro[4.5]decan-8-yl)ethyl)-2-naphthamide 2,2,2-Trifluoroacetate (25a).** 8-(2-Aminoethyl)-1-(4-fluorophenyl)-1,3,8-triazaspiro[4.5]decan-4-one dihydrochloride (34 mg, 0.09 mmol), 2-naphthoyl chloride

(17.8 mg, 0.09 mmol), and *N*,*N*-diisopropylethylamine (0.067 mL, 0.385 mmol) were all dissolved in *N*,*N*-dimethylformamide (1 mL) at 0 °C. The reaction mixture was allowed to warm to room temperature and stirred for about 12 h. The reaction mixture was diluted with water and extracted into dichloromethane 5 times. The dichloromethane layer was then washed 3 times with a solution of lithium chloride (3 M) and dried under reduced pressure. The reaction mixture was subjected to reversed-phase chromatography to afford a white solid (25.8 mg, 0.04 mmol, 51%). ^{1}H NMR (400.1 MHz, DMSO-d_6) δ (ppm): 9.92 (s, 1H), 9.02 (s, 1H), 8.97 (t, J = 5 Hz, 1H), 8.48 (s, 1H), 8.06−7.94 (m, 4H), 7.66−7.58 (m, 2H), 7.09 (t, J = 9 Hz, 2H), 7.03−6.97 (m, 2H), 4.61 (s, 2H), 3.76−3.63 (m, 6H), 3.38−3.34 (m, 2H), 2.63−2.51 (m, 2H), 1.97 (d, J = 14 Hz, 2H). ^{13}C NMR (100.6 MHz, DMSO-d_6) δ (ppm): 174.7, 166.9, 157.6, 155.3, 139.3, 134.3, 132.1, 131.2, 128.9 (2C), 128.0, 127.8, 127.7 (2C), 126.9, 124.1, 118.2, 118.1, 115.7, 115.5, 59.2, 56.7, 55.3, 50.0 (2C), 34.6, 26.5 (2C). HRMS (TOF, ESI) $C_{26}H_{28}N_4O_2F$ $[M + H]^+$ calculated 447.2196, found 447.2196. LC-MS: rt (min) = 2.140. LRMS (ESI) m/z = 447.2. Analogues **25b−d** were made following the same protocol starting from **21d** and were purified via reversed-phase chromatography to greater than 95% purity (as trifluoroacetate salts) as analyzed by ELSD and UV at both 214 and 254 nM.

8-(2-Aminoethyl)-1-(4-chlorophenyl)-1,3,8-triazaspiro[4.5]decan-4-one Dihydrochloride (21e). 1-(4-Chlorophenyl)-1,3,8-triazaspiro[4.5]decan-4-one **20e** (152 mg, 0.57 mmol) and *tert*-butyl (2-oxoethyl)carbamate (100 mg, 0.63 mmol) were combined and dissolved in dichloromethane (1.5 mL) and methanol (0.05 mL) and stirred for about 30 min at room temperature. After about 30 min macroporous triacetoxyborohydride (600 mg, 1.4 mmol) was added to the reaction, and after 14 h an additional amount of *tert*-butyl (2-oxoethyl)carbamate (76 mg, 0.32 mmol) was added to drive the reaction to completion. After about 24 h the reaction mixture was filtered through Celite and concentrated under reduced pressure. The crude compound was chromatographed on a 12 g flash column eluting in a gradient of 0%−10% methanol in dichloromethane to afford a white solid (108 mg, 0.26 mmol, 46%). ^{1}H NMR (400.1 MHz, MeOD) δ (ppm): 7.23 (d, J = 9 Hz, 2H), 6.96 (d, J = 9 Hz, 2H), 4.69 (s, 2H), 3.39−3.32 (m, 2H), 3.26−3.17 (m, 2H), 2.90−2.83 (m, 2H), 2.78−2.67 (m, 2H), 1.97 (s, 2H), 1.84 (d, J = 14 Hz, 2H), 1.45 (s, 9H). ^{13}C NMR (100.6 MHz, MeOD) δ (ppm): 178.0, 158.5, 143.1, 130.1 (2C), 125.4, 118.1 (2C), 80.5, 60.6, 59.6, 58.2, 50.6 (2C), 37.6, 28.8 (2C), 28.7 (3C). HRMS (TOF, ESI) $C_{20}H_{30}N_4O_3Cl$ $[M + H]^+$ calculated 409.2006, found 409.2006. LC-MS: rt (min) = 2.002. LRMS (ESI) m/z = 409.2. *tert*-Butyl (2-(1-(4-chlorophenyl)-4-oxo-1,3,8-triazaspiro[4.5]decan-8-yl)ethyl)carbamate (108 mg, 0.26 mmol) was dissolved in dichloromethane (5 mL) and a minimal amount of methanol added dropwise. Hydrochloric acid was added (4 M in dioxane, 1.5 mL), and the reaction was stirred for approximately 16 h at room temperature. The reaction was concentrated under reduced pressure to afford a white solid (94 mg, 0.25 mmol, 95%). ^{1}H NMR (400.1 MHz, MeOD) δ (ppm): 7.25 (d, J = 9 Hz, 2H), 7.06 (d, J = 9 Hz, 2H), 4.73 (s, 2H), 3.95−3.85 (m, 2H), 3.72−3.64 (m, 2H), 3.51 (s, 4H), 3.19−3.08 (m, 2H), 2.03 (d, J = 15 Hz, 2H). ^{13}C NMR (100.6 MHz, MeOD) δ (ppm): 177.1, 142.5, 130.3 (2C), 125.3, 117.5 (2C), 60.6, 58.4, 55.0, 51.3 (2C), 35.5, 27.8 (2C). HRMS (TOF, ESI) $C_{15}H_{22}N_4OCl$ $[M + H]^+$ calculated 309.1482, found 309.1479. LC-MS: rt (min) = 1.420. LRMS (ESI) m/z = 309.1.

***N*-(2-(1-(4-Chlorophenyl)-4-oxo-1,3,8-triazaspiro[4.5]decan-8-yl)ethyl)-2-naphthamide 2,2,2-Trifluoroacetate (26a).** 8-(2-Aminoethyl)-1-(4-chlorophenyl)-1,3,8-triazaspiro[4.5]decan-4-one dihydrochloride **21e** (94 mg, 0.24 mmol), 2-naphthoyl chloride (47.1 mg, 0.24 mmol), and *N*,*N*-diisopropylethylamine (0.182 mL, 1.05 mmol) were all dissolved in *N*,*N*-dimethylformamide (1 mL) at 0 °C. The reaction mixture was allowed to warm to room temperature and stirred for about 12 h. The reaction mixture was diluted with water and extracted into dichloromethane 5 times. The dichloromethane layer was then washed 3 times with a solution of lithium chloride (3 M) and dried under reduced pressure. The reaction mixture was subjected to reversed-phase chromatography to afford a white solid (62.9 mg, 0.11 mmol, 45%). ^{1}H NMR (400.1 MHz, DMSO-d_6) δ (ppm): 10.24 (s, 1H), 9.10 (s, 1H), 9.01 (t, J = 5 Hz, 1H), 8.49 (s, 1H), 8.06−7.94 (m, 4H), 7.65−7.57 (m,2 H), 7.23 (d, J = 9 Hz, 2H), 6.94 (d, J = 9 Hz, 2H), 4.63 (s, 2H), 3.78−3.65 (m, 6H), 3.40−3.33 (m, 2H), 2.85−2.72 (m, 2H), 1.96 (d, J = 14 Hz, 2H). ^{13}C NMR (100.6 MHz, DMSO-d_6) δ (ppm): 174.5, 166.9, 158.9, 141.7, 134.3, 132.1, 131.2, 128.9 (2C), 128.7 (2C), 128.0 (2C), 127.8, 127.7 (2C), 126.8, 124.1, 122.1, 115.7, 59.0, 56.5, 55.2, 48.9 (2C), 34.6, 26.0 (2C). HRMS (TOF, ESI) HRMS (TOF, ESI) $C_{26}H_{28}N_4O_2Cl$ $[M + H]^+$ calculated 463.1901, found 463.1897. LC-MS: rt (min) = 2.249. LRMS (ESI) m/z = 463.2. Analogues **26b−d** were made following the same protocol starting from **21e** and were purified via reversed-phase chromatography to greater than 95% purity (as trifluoroacetate salts) as analyzed by ELSD and UV at both 214 and 254 nM.

8-(2-Aminoethyl)-1-(4-bromophenyl)-1,3,8-triazaspiro[4.5]decan-4-one Dihydrochloride (21f). 1-(4-Bromophenyl)-1,3,8-triazaspiro[4.5]decan-4-one **20f** (177 mg, 0.57 mmol) and *tert*-butyl (2-oxoethyl)carbamate (100 mg, 0.63 mmol) were combined and dissolved in dichloromethane (1.5 mL) and methanol (0.05 mL) and stirred for about 30 min at room temperature. After about 30 min macroporous triacetoxyborohydride (600 mg, 1.4 mmol) was added to the reaction, and after 14 h an additional amount of *tert*-butyl (2-oxoethyl)carbamate (76 mg, 0.32 mmol) was added to drive the reaction to completion. After about 24 h the reaction mixture was filtered through Celite and concentrated under reduced pressure. The crude compound was chromatographed on a 12 g flash column eluting in a gradient of 0%−10% methanol in dichloromethane to afford a white solid (163 mg, 0.36 mmol, 63%). ^{1}H NMR (400.1 MHz, MeOD) δ (ppm): 7.35 (d, J = 9 Hz, 2H), 6.90 (d, J = 9 Hz, 2H), 4.68 (s, 2H), 3.29−3.21 (m, 2H), 3.20−3.10 (m, 2H), 2.86−2.68 (m, 4H), 1.97 (s, 2H), 1.80 (d, J = 14 Hz, 2H), 1.45 (s, 9H). ^{13}C NMR (100.6 MHz, MeOD) δ (ppm): 176.2, 155.6, 143.4, 129.0 (2C), 117.6, 114.3 (2C), 77.5, 58.6, 58.2, 57.4, 49.3 (2C), 37.7, 28.3 (2C), 28.3 (3C). HRMS (TOF, ESI) $C_{20}H_{30}N_4O_3Br$ $[M + H]^+$ calculated 453.1501, found 453.1504. LC-MS: rt (min) = 2.048. LRMS (ESI) m/z = 455.1. *tert*-Butyl (2-(1-(4-bromophenyl)-4-oxo-1,3,8-triazaspiro[4.5]decan-8-yl)ethyl)carbamate (163 mg, 0.35 mmol) was dissolved in dichloromethane (5 mL) and a minimal amount of methanol added dropwise. Hydrochloric acid was added (4 M in dioxane, 1.5 mL), and the reaction was stirred for approximately 16 h at room temperature. The reaction was concentrated under reduced pressure to afford a white solid (140 mg, 0.33 mmol, 94%). ^{1}H NMR (400.1 MHz, DMSO-d_6) δ (ppm): 9.09 (s, 1H), 8.48 (br s, 2H), 7.29 (d, J = 9 Hz, 2H), 7.09 (d, J = 9 Hz, 2H), 4.61 (s, 2H), 3.71−3.58 (m, 4H), 3.47−3.38 (m, 4H), 3.09−2.97 (m, 2H), 1.89 (d, J = 14 Hz, 2H). ^{13}C NMR (100.6 MHz, DMSO-d_6) δ (ppm): 174.5, 141.8, 131.5 (2C), 115.9 (2C), 109.1, 58.9, 56.4, 53.3, 49.2 (2C), 33.7, 25.5 (2C). HRMS (TOF, ESI) $C_{15}H_{22}N_4OBr$ $[M + H]^+$ calculated 353.0977, found 353.0977. LC-MS: rt (min) = 1.467. LRMS (ESI) m/z = 353.1.

***N*-(2-(1-(4-Bromophenyl)-4-oxo-1,3,8-triazaspiro[4.5]decan-8-yl)ethyl)-2-naphthamide 2,2,2-Trifluoroacetate (27a).** 8-(2-Aminoethyl)-1-(4-bromophenyl)-1,3,8-triazaspiro[4.5]decan-4-one dihydrochloride **21f** (66 mg, 0.15 mmol), 2-naphthoyl chloride (29.5 mg, 0.15 mmol), and *N*,*N*-diisopropylethylamine (0.126 mL, 0.73 mmol) were all dissolved in *N*,*N*-dimethylformamide (1 mL) at 0 °C. The reaction mixture was allowed to warm to room temperature and stirred for about 12 h. The reaction mixture was diluted with water and extracted into dichloromethane 5 times. The dichloromethane layer was then washed 3 times with a solution of lithium chloride (3 M) and dried under reduced pressure. The reaction mixture was subjected to reversed-phase chromatography to afford a white solid

(66.1 mg, 0.11 mmol, 71%). ^{1}H NMR (400.1 MHz, DMSO-d_6) δ (ppm): 10.23 (s, 1H), 9.10 (s, 1H), 9.00 (t, J = 5 Hz, 1H), 8.49 (s, 1H), 8.06−7.93 (m, 4H), 7.65−7.58 (m, 2H), 7.34 (d, J = 9 Hz, 2H), 6.89 (d, J = 9 Hz, 2H), 4.62 (s, 2H), 3.78−3.66 (m, 6H), 3.46−3.40 (m, 2H), 2.86−2.74 (m, 2H), 1.95 (d, J = 14 Hz, 2H). ^{13}C NMR (100.6 MHz, DMSO-d_6) δ (ppm): 174.5, 166.9, 158.9, 142.1, 134.3, 132.1, 131.6 (2C), 131.2, 128.9 (2C), 128.0 (2C), 127.8, 127.7 (2C), 126.8, 124.1, 116.1, 109.6, 58.9, 56.5, 55.2, 48.9 (2C), 34.6, 25.9 (2C). HRMS (TOF, ESI) $C_{26}H_{28}N_4O_2Br$ $[M + H]^+$ calculated 507.1396, found 507.1393. LC-MS: rt (min) = 2.279. LRMS (ESI) m/z = 507.1. Analogues **27b**−**d** were made following the same protocol starting from **21f** and were purified via reversed-phase chromatography to greater than 95% purity (as trifluoroacetate salts) as analyzed by ELSD and UV at both 214 and 254 nM.

(*S*)-*tert*-Butyl (1-(1-(3-Fluorophenyl)-4-oxo-1,3,8-triazaspiro-[4.5]decan-8-yl)propan-2-yl)carbamate (29). 1-(3-Fluorophenyl)-1,3,8-triazaspiro[4.5]decan-4-one **20a** (366 mg, 1.46 mmol) and (*S*)-*tert*-butyl (1-oxopropan-2-yl)carbamate (356 mg, 2.00 mmol) were combined and dissolved in dichloromethane (10 mL) and methanol (1 mL) and stirred for about 30 min at room temperature. After about 30 min macroporous triacetoxyborohydride (2 g, 4.84 mmol) was added to the reaction. After about 24 h the reaction mixture was filtered through Celite and concentrated under reduced pressure. The crude compound was chromatographed on an 80 g flash column eluting in a gradient of 0%−10% methanol in dichloromethane to afford a white solid (191 mg, 0.47 mmol, 34%). ^{1}H NMR (400.1 MHz, MeOD) δ (ppm): 7.23 (q, J = 8 Hz, 1H), 6.76−6.68 (m, 2H), 6.55−6.49 (m, 1H), 4.69 (s, 2H), 3.96−3.84 (m, 1H), 3.25−3.07 (m, 2H), 2.90−2.63 (m, 4H), 1.96 (s, 2H), 1.79 (d, J = 14 Hz, 2H), 1.46 (s, 9H), 1.18 (d, J = 7 Hz, 3H). ^{13}C NMR (100.6 MHz, MeOD) δ (ppm): 178.2, 164.0, 158.3, 146.2, 131.6, 111.3, 105.7, 102.4, 80.5, 64.2, 60.5 (2C), 59.8, 51.5, 50.5, 28.9 (2C), 28.7 (3C), 19.6. HRMS (TOF, ESI) $C_{21}H_{32}N_4O_3F$ $[M + H]^+$ calculated 407.2458, found 407.2449. LC-MS: rt (min) = 1.932. LRMS (ESI) m/z = 407.2.

(*S*)-8-(2-Aminopropyl)-1-(3-fluorophenyl)-1,3,8-triazaspiro-[4.5]decan-4-one Dihydrochloride (30). (*S*)-*tert*-Butyl (1-(1-(3-fluorophenyl)-4-oxo-1,3,8-triazaspiro[4.5]decan-8-yl)propan-2-yl)carbamate **29** (166 mg, 0.40 mmol) was dissolved in dichloromethane (15 mL) and a minimal amount of methanol added dropwise. Hydrochloric acid was added (4 M in dioxane, 2.0 mL), and the reaction was stirred for approximately 16 h at room temperature. The reaction was concentrated under reduced pressure to afford a light tan solid (150 mg, 0.39 mmol, 98%). ^{1}H NMR (400.1 MHz, DMSO-d_6) δ (ppm): 9.12 (s, 1H), 8.63 (s, 2H), 7.22−7.12 (m, 1H), 7.08−7.01 (m, 1H), 6.79−6.72 (m, 1H), 6.56−6.49 (m, 1H), 4.62 (s, 2H), 3.95−3.58 (m, 4H), 3.54−3.41 (m, 3H), 3.15−3.00 (m, 2H), 1.89 (d, J = 14 Hz, 2H), 1.32 (d, J = 5 Hz, 3H). ^{13}C NMR (100.6 MHz, DMSO-d_6) δ (ppm): 174.3, 162.1, 144.4, 130.2, 109.8, 103.9, 100.5, 59.4, 58.9, 56.5, 50.5, 48.5, 42.4, 25.7, 25.5, 17.1. HRMS (TOF, ESI) $C_{16}H_{24}N_4OF$ $[M + H]^+$ calculated 307.1934, found 307.1934. LC-MS: rt (min) = 0.255. LRMS (ESI) m/z = 307.1.

(*S*)-*N*-(1-(1-(3-Fluorophenyl)-4-oxo-1,3,8-triazaspiro[4.5]decan-8-yl)propan-2-yl)-2-naphthamide 2,2,2-Trifluoroacetate (31). (*S*)-8-(2-Aminopropyl)-1-(3-fluorophenyl)-1,3,8-triazaspiro[4.5]decan-4-one dihydrochloride **30** (140 mg, 0.37 mmol), 2-naphthoyl chloride (76 mg, 0.40 mmol), and *N*,*N*-diisopropylethylamine (0.225 mL, 1.29 mmol) were all dissolved in *N*,*N*-dimethylformamide (5 mL) at 0 °C. The reaction mixture was allowed to warm to room temperature and stirred for about 12 h. The reaction mixture was diluted with water and extracted into dichloromethane 5 times. The dichloromethane layer was then washed 3 times with a solution of lithium chloride (3 M) and dried under reduced pressure. The reaction mixture was subjected to reversed-phase chromatography to afford a white solid (19.3 mg, 0.03 mmol, 9%). ^{1}H NMR (400.1 MHz, DMSO-d_6) δ (ppm): 9.74 (s, 1H), 9.10 (s, 1H), 8.78 (d, J = 8 Hz, 1H), 8.50 (s, 1H), 8.06−7.95 (m, 4H), 7.66−7.58 (m, 2H), 7.20 (q, J = 8 Hz, 1H), 6.76−6.69 (m, 2H), 6.60−6.53 (m, 1H), 4.62 (s, 2H), 3.88−3.69 (m, 3H), 3.61−3.54 (m, 1H), 3.43−3.33 (m, 3H), 2.93−2.71 (m, 2H), 2.01−1.82 (m, 2H), 1.31 (d, J = 7 Hz, 3H). ^{13}C NMR (100.6 MHz, DMSO-d_6) δ (ppm): 174.4, 166.7, 162.1, 144.7, 134.3, 132.1, 131.4, 130.6, 130.5, 128.9, 127.9 (2C), 127.8 (2C), 127.7, 126.9, 124.4, 109.8, 104.3, 100.9, 60.8, 59.0, 56.6, 49.8, 48.7, 41.3, 26.0, 25.8, 19.0. HRMS (TOF, ESI) $C_{27}H_{30}N_4O_2F$ $[M + H]^+$ calculated 461.2353, found 461.2354. LC-MS: rt (min) = 0.445. LRMS (ESI) m/z = 461.2.

Pharmacology Methods. Cell Culture. Calu-1 and MDA-231 cells were purchased from American Type Culture Collection (Manassas, VA). Calu-1 and MDA-231 cells were maintained in DMEM supplemented with 10% FBS, 100 μg/mL penicillin−streptomycin, and 0.25 μg/mL amphotericin. HEK293 cells stably expressing GFP-tagged human PLD2A were generated in the laboratory. To sustain selection pressure low-passage-number HEK293-gfpPLD2 cells were maintained in DMEM supplemented with 10% FBS, 100 μg/mL penicillin−streptomycin, 2 μg/mL puromycin, and 600 μg/mL G418. All HEK293-gfpPLD2 experiments were done on tissue culture plates that had been coated with low levels of polylysine. All cells were maintained in a humidified 5% CO_2 incubator at 37 °C.

Cellular Phospholipase D Activity Assays. PLD1 and PLD2 cellular IC_{50} values were determined as described previously.[26]

Assessment of Cell Proliferation via WST-1 Assay. Cells are plated into 96-well tissue culture plates at 15000 cells/well in tissue culture treated 96-well black wall/clear bottom assay plates (Corning Inc. Costar plates) in complete growth medium and allowed to grow overnight. After 24 h of growth media were removed, and cells were treated with PLD inhibitor or DMSO vehicle control in 100 μL of DMEM, 1% AA, ± 10% FBS. Media and inhibitor were replenished every 24 h, and after 48 h cells were treated with 10 μL/well of a modified MTT reagent, WST-1 cell proliferation reagent (Roche Diagnostics Corp., Indianapolis, IN). Plates were then incubated for 1 h at 37 °C. After incubation UV absorbance was measured at 450 nm with a BioTek Synergy HT plate reader (BioTek Inc., Winooski, VT). Background signal was subtracted from wells with no cells present. Data are expressed as absorbance at 450 nm.

For time course experiments cells were seeded at 7500 cells/well into media containing PLD inhibitor or DMSO vehicle control. Media were removed and replaced every 24 h, and at set time points (24, 48, 72, and 96 h) cells were treated with WST-1 reagent as described above.

Assessment of Caspase 3/7 Activity. Caspase 3/7 activity was measured using a homogeneous bioluminescent method according to manufacturer's directions (Caspase-Glo 3/7 assay; Promega, Madison, WI). In this assay, caspase 3/7 activity is measured by the ability to cleave the proluminescent Caspase 3/7 specific DEVD-aminoluciferin substrate to liberate the free aminoluciferin which is then consumed by luciferase generating a luminescent signal. The luminescent signal is directly proportional to the amount of Caspase 3/7 activity. Cells were plated at 15000 cells/well in tissue culture treated 96-well black wall/clear bottom assay plates (Corning Inc. Costar plates) in 50 μL of growth medium at 37 °C. After 24 h media were removed and replaced with DMEM, 1% AA, ± 10% FBS with either PLD inhibitor or DMSO vehicle control. Media were replenished every 24 h to account for metabolism of the compounds. After 48 h growth in the presence of PLD inhibitor 50 μL Caspase-Glo 3/7 reagent was added to each well, plates were incubated at room temperature for 1 h, and luminescent signal was then detected with a BioTek Synergy HT plate reader (BioTek Inc., Winooski, VT). Caspase 3/7 activity was normalized to vehicle control and expressed as fold stimulation of Caspase activity.

Pharmacokinetic Studies. (A) In Vitro. The metabolism of PLD inhibitors **14** and **22a** was investigated in rat hepatic microsomes (BD Biosciences, Billerica, MA) using substrate depletion methodology (percent test article remaining). A potassium phosphate-buffered reaction mixture (0.1 M, pH 7.4) of test article (1 μM) and microsomes (0.5 mg/mL) was preincubated

(5 min) at 37 °C prior to the addition of NADPH (1 mM). The incubations, performed in 96-well plates, were continued at 37 °C under ambient oxygenation, and aliquots (80 μL) were removed at selected time intervals (0, 3, 7, 15, 25, and 45 min). Protein was precipitated by the addition of chilled acetonitrile (160 μL), containing glyburide as an internal standard (50 ng/mL), and centrifuged at 3000 rpm (4 °C) for 10 min. Resulting supernatants were transferred to new 96-well plates in preparation for LC-MS-MS analysis. The in vitro half-life ($t_{1/2}$, min, eq 1), intrinsic clearance (CL_{int}, mL min^{-1} kg^{-1}, eq 2), and subsequent predicted hepatic clearance (CL_{hep}, mL min^{-1} kg^{-1}, eq 3) were determined employing the equations:

$$t_{1/2} = \ln(2)/k \quad (1)$$

where k represents the slope from linear regression analysis (percent test article remaining)

$$CL_{int} = (0.693/t_{1/2})(\text{reaction volume/mg of microsomes}) \times (45 \text{ mg of microsomes/g of liver}) \times (20 \text{ g of liver/kg body weight}) \quad (2)$$

with scale-up factors of 20 (human) and 45 (rat)

$$CL_{hep} = \frac{Q(CL_{int})}{Q + CL_{int}} \quad (3)$$

(B) In Vivo. Male Sprague-Dawley rats (n = 2) weighing around 300 g were purchased from Harlon Laboratories (Indianapolis, IN) and implanted with catheters in the carotid artery and jugular vein. The cannulated animals were acclimated to their surroundings for approximately 1 week before dosing and provided food and water ad libitum. Compounds **14** and **22a** were administered intravenously (iv) to rats via the jugular vein catheter in 20% DMSO/80% saline at a dose of 1 mg/kg and a dose volume of 1 mL/kg. Blood collections via the carotid artery were performed at predose and at 2 min, 7 min, 15 min, 30 min, and 1 h, 2 h, 4 h, 7 h, and 24 h postdose. Samples were collected into chilled, EDTA-fortified tubes and centrifuged for 10 min at 3000 rpm (4 °C), and resulting plasma was aliquoted into 96-well plates for LC-MS-MS analysis. All pharmacokinetic analysis was performed employing noncompartmental analysis. For oral exposure studies, measuring both systemic plasma and CNS tissue exposure, compounds **14** and **22a** were administered (oral gavage) to fasted rats (n = 2) as suspensions in 10% Tween 80/0.5% methylcellulose at a dose of 10 mg/kg and in a dosing volume of 10 mL/kg; blood and whole brain samples were collected at 1.5 h postdose. Blood was collected into chilled, EDTA-fortified tubes, centrifuged for 10 min at 3000 rpm (4 °C), and stored at −80 °C until LC-MS-MS analysis. The brain samples were rinsed in PBS, snap-frozen, and stored at −80 °C. Prior to LC-MS-MS analysis, brain samples were thawed to room temperature and subjected to mechanical homogenation employing a Mini-Beadbeater and 1.0 mm zirconia/silica beads (BioSpec Products). All animal studies were approved by the Vanderbilt University Medical Center Institutional Animal Care and Use Committee. The animal care and use program is fully accredited by the Association for Assessment and Accreditation of Laboratory Animal Care, International.

Plasma Protein Binding. Protein binding of the PLD inhibitors **14** and **22a** was determined in rat plasma via equilibrium dialysis employing Single-Use RED Plates with inserts (ThermoFisher Scientific, Rochester, NY). Briefly, plasma (220 μL) was added to the 96-well plate containing test article (5 μL) and mixed thoroughly. Subsequently, 200 μL of the plasma test article mixture was transferred to the *cis* chamber (red) of the RED plate, with an accompanying 350 μL of phosphate buffer (25 mM, pH 7.4) in the *trans* chamber. The RED plate was sealed and incubated 4 h at 37 °C with shaking. At completion, 50 μL aliquots from each chamber were diluted 1:1 (50 μL) with either plasma (*cis*) or buffer (*trans*) and transferred to a new 96-well plate, at which time ice-cold acetonitrile (2 volumes) was added to extract the matrices. The plate was centrifuged (3000 rpm, 10 min), and supernatants were transferred to a new 96-well plate. The sealed plate was stored at −20 °C until LC-MS-MS analysis.

Liquid Chromatography/Mass Spectrometry Analysis. (A) In Vivo Experiments. PLD inhibitors **14** and **22a** were analyzed via electrospray ionization (ESI) on an AB Sciex API-4000 (Foster City, CA) triple-quadrupole instrument that was coupled with Shimadzu LC-10AD pumps (Columbia, MD) and a Leap Technologies CTC PAL autosampler (Carrboro, NC). Analytes were separated by gradient elution using a Fortis C18 2.1 × 50 mm, 3.5 μm column (Fortis Technologies Ltd., Cheshire, U.K.) thermostated at 40 °C. HPLC mobile phase A was 0.1% NH_4OH (pH unadjusted); mobile phase B was acetonitrile. The gradient started at 30% B after a 0.2 min hold and was linearly increased to 90% B over 0.8 min, held at 90% B for 0.5 min, and returned to 30% B in 0.1 min followed by a reequilibration (0.9 min). The total run time was 2.5 min, and the HPLC flow rate was 0.5 mL/min. The source temperature was set at 500 °C, and mass spectral analyses were performed using multiple reaction monitoring (MRM), with transitions for **14** (m/z 497.5 → 202.3) and **22a** (m/z 447.4 → 198.1) utilizing a Turbo-Ionspray source in positive ionization mode (5.0 kV spray voltage). All data were analyzed using AB Sciex Analyst 1.4.2 software.

(B) In Vitro Experiments. The PLD inhibitors were analyzed similarly to that described above (In Vivo Experiments) with the following exceptions: LC-MS-MS analysis was performed employing a TSQ Quantum^{ULTRA} that was coupled to a Thermo-Surveyor LC system (Thermoelectron Corp., San Jose, CA) and a Leap Technologies CTC PAL autosampler (Carrboro, NC). Chromatographic separation of analytes was achieved with an Acquity BEH C18 2.1 × 50 mm, 1.7 μm column (Waters, Taunton, MA).

Acknowledgment. R.R.L. was supported by an NIH integrative training in therapeutic discovery training grant (T90DA022873). H.A.B. and C.W.L. were supported by the John S. McDonnell Foundation. The authors thank Katrina Brewer and Matthew Mulder for in vitro drug metabolism stability and protein binding data.

References

(1) American Cancer Society. Cancer Facts & Figures 2009.
(2) Brown, H. A.; Henage, L. G.; Preininger, A. M.; Xiang, Y.; Exton, J. H. Biochemical analysis of phospholipase D. *Methods Enzymol.* **2007**, *434*, 49–87.
(3) Foster, D. A. Phosphatidic acid signaling to mTOR: Signals for the survival of human cancer cells. *Biochim. Biophys. Acta* **2009**, *1791*, 949–955.
(4) Noh, D. Y. Overexpression of phospholipase D1 in human breast cancer tissues. *Cancer Lett.* **2000**, *161*, 207–214.
(5) Zhao, Y.; Ehara, H.; Akao, Y.; Shamoto, M.; Nakagawa, Y.; Banno, Y.; Deguchi, T.; Ohishi, N.; Yagi, K.; Nozawa, Y. Increased activity and intranuclear expression of phospholipase D2 in human renal cancer. *Biochem. Biophys. Res. Commun.* **2000**, *278*, 140–143.
(6) Yamada, Y. Association of a polymorphism of the phospholipase D2 gene with the prevalence of colorectal cancer. *J. Mol. Med.* **2003**, *81*, 126–131.
(7) Park, M. H.; Ahn, B. H.; Hong, Y. K.; Min, D. S. Overexpression of phospholipase D enhances matrix metalloproteinase-2 expression and glioma cell invasion via protein kinase C and protein kinase A/NF-kappa B/Sp1-mediated signaling pathways. *Carcinogenesis* **2009**, *30*, 356–365.
(8) Buchanan, F. G.; McReynolds, M.; Couvillon, A.; Kam, Y.; Holla, V. R.; DuBois, R. N.; Exton, J. H. Requirement of phospholipase D1 activity in H-Ras(V12)-induced transformation. *Proc. Natl. Acad. Sci. U.S.A.* **2005**, *102*, 1638–1642.

(9) Zheng, Y.; Rodrik, V.; Toschi, A.; Shi, M.; Hui, L.; Shen, Y.; Foster, D. A. Phospholipase D couples survival and migration signals in stress response of human cancer cells. *J. Biol. Chem.* **2006**, *281*, 15862–15868.
(10) Shi, M.; Zheng, Y.; Garcia, A.; Xu, L.; Foster, D. A. Phospholipase D provides a survival signal in human cancer cells with activated H-Ras or K-Ras. *Cancer Lett* **2007**, *258*, 268–275.
(11) Snider, A. J.; Zhang, Z. H.; Xie, Y. H.; Meier, K. E. Epidermal growth factor increases lysophosphatidic acid production in human ovarian cancer cells: roles for phospholipase D-2 and receptor transactivation. *Am. J. Physiol.* **2010**, *298*, C163–C170.
(12) Williger, B. T.; Ho, W. T.; Exton, J. H. Phospholipase D mediates matrix metalloproteinase-9 secretion in phorbol ester-stimulated human fibrosarcoma cells. *J. Biol. Chem.* **1999**, *274*, 735–738.
(13) Hui, L.; Zheng, Y.; Yan, Y.; Bargonetti, J.; Foster, D. A. Mutant p53 in MDA-MB-231 breast cancer cells is stabilized by elevated phospholipase D activity and contributes to survival signals generated by phospholipase D. *Oncogene* **2006**, *25*, 7305–7310.
(14) Hui, L.; Abbas, T.; Pielak, R. M.; Joseph, T.; Bargonetti, J.; Foster, D. A. Phospholipase D elevates the level of MDM2 and suppresses DNA damage-induced increases in p53. *Mol. Cell. Biol.* **2004**, *24*, 5677–5686.
(15) Chen, Y.; Rodrik, V.; Foster, D. A. Alternative phospholipase D/mTOR survival signal in human breast cancer cells. *Oncogene* **2005**, *24*, 672–679.
(16) Hui, L.; Rodrik, V.; Pielak, R. M.; Knirr, S.; Zheng, Y.; Foster, D. A. mTOR-dependent suppression of protein phosphatase 2A is critical for phospholipase D survival signals in human breast cancer cells. *J. Biol. Chem.* **2005**, *280*, 35829–35835.
(17) Zhao, C. Phospholipase D2-generated phosphatidic acid couples EGFR stimulation to Ras activation by Sos. *Nat. Cell Biol.* **2007**, *9*, 706–712.
(18) Tou, J. S.; Urbizo, C. Diethylstilbestrol inhibits phospholipase D activity and degranulation by stimulated human neutrophils. *Steroids* **2008**, *73*, 216–221.
(19) Tou, J. S.; Urbizo, C. Resveratrol inhibits the formation of phosphatidic acid and diglyceride in chemotactic peptide- or phorbol ester-stimulated human neutrophils. *Cell. Signalling* **2001**, *13*, 191–197.
(20) Garcia, A.; Zheng, Y.; Zhao, C.; Toschi, A.; Fan, J.; Shraibman, N.; Brown, H. A.; Bar-Sagi, D.; Foster, D. A.; Arbiser, J. L. Honokiol suppresses survival signals mediated by Ras-dependent phospholipase D activity in human cancer cells. *Clin. Cancer Res.* **2008**, *14*, 4267–4274.
(21) Puar, M. S.; Barrabee, E.; Hallade, M.; Patel, M. Sch 420789: A novel fungal metabolite with phospholipase D inhibitory activity. *J. Antibiot.* **2000**, *53*, 837–838.
(22) McDonald, L. A.; Barbieri, L. R.; Bernan, V. S.; Janso, J.; Lassota, P.; Carter, G. T. 07H239-A, a new cytotoxic eremophilane sesquiterpene from the marine-derived xylariaceous fungus LL-07H239. *J. Nat. Prod.* **2004**, *67*, 1565–1567.
(23) Levy, B. D.; Hickey, L.; Morris, A. J.; Larvie, M.; Keledjian, R.; Petasis, N. A.; Bannenberg, G.; Serhan, C. N. Novel polyisoprenyl phosphates block phospholipase D and human neutrophil activation in vitro and murine peritoneal inflammation in vivo. *Br. J. Pharmacol.* **2005**, *146*, 344–351.
(24) Eisen, S. F.; Brown, H. A. Selective estrogen receptor (ER) modulators differentially regulate phospholipase D catalytic activity in ER-negative breast cancer cells. *Mol. Pharmacol.* **2002**, *62*, 911–20.
(25) Monovich, L.; Mugrage, B.; Quadros, E.; Toscano, K.; Tommasi, R.; LaVoie, S.; Liu, E.; Du, Z. M.; LaSala, D.; Boyar, W.; Steed, P. Optimization of halopemide for phospholipase D2 inhibition. *Bioorg. Med. Chem. Lett.* **2007**, *17*, 2310–2311.
(26) Scott, S. A.; Selvy, P. E.; Buck, J. R.; Cho, H. P.; Criswell, T. L.; Thomas, A. L.; Armstrong, M. D.; Arteaga, C. L.; Lindsley, C. W.; Brown, H. A. Design of isoform-selective phospholipase D inhibitors that modulate cancer cell invasiveness. *Nat. Chem. Biol.* **2009**, *5*, 108–117.
(27) Lewis, J. A.; Scott, S. A.; Lavieri, R.; Buck, J. R.; Selvy, P. E.; Stoops, S. L.; Armstrong, M. D.; Brown, H. A.; Lindsley, C. W. Design and synthesis of isoform-selective phospholipase D (PLD) inhibitors. Part I: Impact of alternative halogenated privileged structures for PLD1 specificity. *Bioorg. Med. Chem. Lett.* **2009**, *19*, 1916–1920.
(28) Lavieri, R.; Scott, S. A.; Lewis, J. A.; Selvy, P. E.; Armstrong, M. D.; Alex Brown, H.; Lindsley, C. W. Design and synthesis of isoform-selective phospholipase D (PLD) inhibitors. Part II: Identification of the 1,3,8-triazaspiro[4,5]decan-4-one privileged structure that engenders PLD2 selectivity. *Bioorg. Med. Chem. Lett.* **2009**, *19*, 2240–2243.
(29) Oliveira, T. G.; Di Paolo, G. Phospholipase D in brain function and Alzheimer's disease. *Biochim. Biophys. Acta* **2010**, *1801*, 799–805.
(30) Jin, J. K.; Ahn, B. H.; Na, Y. J.; Kim, J. I.; Kim, Y. S.; Choi, E. K.; Ko, Y. G.; Chung, K. C.; Kozlowski, P. B.; Mindo, S. Phospholipase D1 is associated with amyloid precursor protein in Alzheimer's disease. *Neurobiol. Aging* **2007**, *28*, 1015–1027.
(31) Elvers, M.; Stegner, D.; Hagedorn, I.; Kleinschnitz, C.; Braun, A.; Kuijpers, M. E.; Boesl, M.; Chen, Q.; Heemskerk, J. W.; Stoll, G.; Frohman, M. A.; Nieswandt, B. Impaired alpha(IIb)beta(3) integrin activation and shear-dependent thrombus formation in mice lacking phospholipase D1. *Sci. Signal.* **2010**, *3*, ra1.